CALCULATION OF COLLISIONAL CROSS SECTIONS FOR THE $^2P_{3/2} \rightarrow {}^2P_{1/2}$ TRANSITION IN ALKALI-NOBLE GAS SYSTEMS

THESIS

Sam Butler, Captain, USAF
AFIT/GAP/ENP/10-M04

DEPARTMENT OF THE AIR FORCE
AIR UNIVERSITY

AIR FORCE INSTITUTE OF TECHNOLOGY

Wright-Patterson Air Force Base, Ohio

The views expressed in this thesis are those of the author and do not reflect the official policy or position of the United States Air Force, Department of Defense, or the United States Government.

AFIT/GAP/ENP/10-M04

CALCULATION OF COLLISIONAL CROSS SECTIONS FOR THE $^2P_{3/2} \rightarrow {}^2P_{1/2}$ TRANSITION IN ALKALI-NOBLE GAS SYSTEMS

THESIS

Presented to the Faculty

Department of Engineering Physics

Graduate School of Engineering and Management

Air Force Institute of Technology

Air University

Air Education and Training Command

in Partial Fulfillment of the Requirements for the

Degree of Master of Science in Applied Physics

Sam Butler, BS

Captain, USAF

March 2010

AFIT/GAP/ENP/10-M04

CALCULATION OF COLLISIONAL CROSS SECTIONS FOR THE $^2P_{3/2} \rightarrow {}^2P_{1/2}$ TRANSITION IN ALKALI-NOBLE GAS SYSTEMS

Sam Butler, BS
Captain, USAF

Approved:

//SIGNED//	
David E. Weeks, PhD (Chairman)	Date
//SIGNED//	
Glen P. Perram, PhD (Member)	Date
//SIGNED//	
William F. Bailey, PhD (Member)	Date

AFIT/GAP/ENP/10-M04

Abstract

Collisional cross sections were calculated as a function of energy for two coupled one dimensional, spherically symmetric potentials. The Split Operator Method[4] was used to propagate an initial Møller state, chosen to be a Gaussian in the asymptotic limit, through a potential. The correlation between the wave packet and Møller final state was calculated at each time step. Using the Channel Packet Method[18], the correlation function was used to obtain scattering matrix elements. From scattering matrix elements for several different effective potential values and using the Method of Partial Waves[7], the collisional cross section is calculated for the transition from the $^2P_{3/2}$ to $^2P_{1/2}$ level. This method was applied to LiHe at low energy, with results close to experimentally measured values for Alkali-Noble Gas interactions. Cross sections were also calculated for NaHe, KHe, RbAr, and LiHe-3. An explanation for the low RbAr cross sections from the time dependent calculations is provided.

Acknowledgements

I would like to thank God for the opportunity to live in such a miraculous time, and for creating a universe full of beauty and scientific curiosity. Just when we think we are beginning to understand how things work, God reveals some additional mysteries to man, as is made readily apparent in the discoveries of quantum mechanics upon which this thesis based, and future discoveries yet to be imagined.

I would like to offer heartfelt thanks to my thesis advisor, Dr. David Weeks, for his abundant enthusiasm and superb teaching skills that made learning scattering theory a pleasure. His abundant and deep love of science is only surpassed by his ability to clearly and concisely convey the concepts at a level that is readily understood by all around him. He has truly been an inspiration in my life and greatly enhanced my neverending thirst for knowledge, and I will forever be in his debt for his tremendous service.

I would also like to thank Dr. Glen Perram and Dr. William Bailey for their contributions to this work, and for the manner in which they are able to enlighten my understanding of the complex nature of the universe. Without their support, and the support of the entire physics department, this work would not have been possible.

I would also like to acknowledge my first physics professor, now retired from Twin Falls High School in Twin Falls, Idaho, for inspiring me to pursue physics, and for the physics department at Brigham Young University, and in particular my modern physics, quantum mechanics and computational physics professors, for their continued inspiration and ability to teach with great clarity and understanding.

Let me also acknowledge the inspirational role of historical giants such as Thomas Jefferson and Benjamin Franklin, whose lives are an inspiration to all; their combination of a deep scientific understanding and tact in handling the affairs of this great country are an inspiration to me in the pursuit of not only scientific issues, but also

their relationship to the nation.

I am forever in debt to my mother for instilling in me a lifelong love of learning. Her impact in my life is impossible to overstate. My brothers have been a tremendous inspiration to me as well throughout my life. I would also like to thank my father for instilling in me a love of the field of computing and for the opportunity to gain skills in this area.

Finally, last only in acknowledgements but first in all else, I would like to thank my wife and children for their sincere support, love, and encouragement throughout the long and difficult process of obtaining a masters degree.

Sam Butler

Table of Contents

Page

Page

List of Figures

Figure Page

Figure Page

List of Tables

List of Abbreviations

Abbreviation		Page
DPAL	Diode Pumped Alkali Laser	1
AFIT	Air Force Institute of Technology	4

CALCULATION OF COLLISIONAL CROSS SECTIONS FOR THE $^2P_{3/2} \rightarrow {}^2P_{1/2}$ TRANSITION IN ALKALI-NOBLE GAS SYSTEMS

I. Overview

1.1 Introduction

Collisional cross sections play a fundamental role in atomic and molecular transitions in many systems. They provide a non-radiative source of energy transfer that is particularly important in laser systems [20]. DPALs are one area of interest in the Air Force where collisions are essential to operation of the laser [14]. The energy level diagrams for all alkali atoms are similar in structure, although they differ in exact positioning and separation of the energy levels, and in the shapes of the potentials of the $^2P_{1/2,3/2}$ states which are involved in the collisional relaxation process.

This situation is not unique to DPALs. In many systems, one often arrives at a decision point where several atoms in one column of the periodic table nearly all appear equally suited for a particular task. It is often difficult to forecast which atom will be most effective, but it is difficult to switch atoms in the middle of the experiment, often requiring entirely new systems and significant effort fine-tuning these systems. Although there are generally several factors which influence the decision, often the collisional parameters are important. The theory of collisional cross sections has been an area of intense research over the past several decades, with varying degrees of success. In systems where collisional effects play a substantial role, the method in this thesis may be used to obtain collisional cross sections between two states, given the potentials for each state and the interaction potential. It is hopeful

that determination of collisional cross sections given input potentials of a system may provide a partial answer to this question in systems where collisions play a major role, such as with DPALs [14], or with most chemical physics interactions.

1.2 Background

In order to calculate collisional cross sections between two coupled states, the Channel Packet Method is used [18] [22]. The method employed is Gaussian wave packet propagation through a diabadic surface using the Channel Packet Method[4] to compute S-matrix elements. This involves propagating a Gaussian wave packet forward and backward in time via the Møller operators, then observing the overlap, which is proportional to the scattering matrix element. These scattering matrix elements are then used to determine the collisional cross sections for several energies.

1.2.1 Propagation.

As discussed in Chapter II, the Channel Packet Method is used to propagate a wave packet. At each time step, there are 2 Fourier transforms required per surface (4 total for a 2-state problem). At each time step, the wave packet is projected on to the Møller final state. The initial and final wave packets are judiciously chosen to provide the collisional cross sections within an energy range of interest.

1.2.2 Collisions.

One can represent the interaction between states as an operator $\hat{S}$, known as the scattering operator. This operator is not time-dependent because it is defined as taking reactants from the infinite past ($|\psi_{in}\rangle$) and resulting in products in the infinite future ($|\psi_{out}\rangle$):

$$|\psi_f\rangle = \hat{S}|\psi_i\rangle \tag{1}$$

From this equation, it is obvious that interactions between potentials must be contained in $\hat{S}$. If it is assumed that only inelastic collisions between the two nearest states can cause an interaction between the potentials, the problem of calculating the collisional transition rate between two states is equivalent to the problem of calculating the matrix elements of $\hat{S}$ in a certain basis [6] [21].

In the simplification of allowing only interactions between two neighboring states and a single k value (plane wave), the S-matrix can be understood as a 2x2 matrix. (The S-matrix is simply the representation $\langle k|\hat{S}|k\rangle$[6].) Under these conditions, the S-matrix can be written as:

$$\mathbb{S} = \begin{bmatrix} S_{+k,+k} & S_{+k,-k} \\ S_{-k,+k} & S_{-k,-k} \end{bmatrix} \tag{2}$$

Which wave function is chosen as the initial Møller state, and which wave function is the final Møller state? It is actually up to you to decide, within some rather flexible boundaries. The choice will determine the outputted energies that are not overrun by numerical error, and which scattering matrix element is calculated. This arbitrary choice of wave function is possible because the influence of the expansion coefficients for each k value are removed from the S-matrix element provided the initial Møller state is either entirely in $+k$ space or in $-k$ space, as discussed in Chapter III. Similarly, the final Møller state must be either entirely in $+k$ space or in $-k$ space. For a spherically symmetric problem, the initial Møller state is often in $-k$ space and the final Møller state is often in $+k$ space. If the initial and final Møller states are placed in the asymptotic limit of the potential, Gaussian wave packets may be used.

Table 1. Summary of Atomic Units

Unit Type	Atomic Units	SI Units
Length	1 Bohr	$5.291772108(18) \times 10^{11}$ m
Mass	1 au (of mass)	$9.1093826(16) \times 10^{31}$ kg
Time	1 au (of time)	$2.418884326505(16) \times 10^{17}$ s
$\hbar$	1 au (of angular momentum)	$1.05457168(18) \times 10^{34}$ J s
Energy	1 Hartree	$4.35974417(75) \times 10^{18}$ J
Cross Section	1 Bohr^2	$0.2800285204(49) \times 10^{-16}$ cm^2

1.2.3 Units.

Atomic units are used in this thesis unless otherwise noted. Conversion from atomic units to SI units are summarized in Table 1.

1.3 Problems and Objectives

It was first necessary to code a Gaussian wave packet propagator. Then the correlation function resutls from the propagator were used to implement the Channel Packet Method and obtain scattering matrix elements. Through the Method of Partial Waves[7], the procedure was repeated for several different effective potentials. The resulting S-matrix elements were summed to obtain the collisional cross section for each energy with numerically stable data. The code was verified under several conditions where the solutions to the scattering problem are known. This code was executed using adiabatic potentials for LiHe from another Ph.D. student at AFIT [5]. From these calculations, the following observations were made:

- The most difficult hurdle to overcome in this process is determination of the coupling potential between the two states of the system
- For these systems, the effective potential died off very slowly for $l \approx l_{max}$. This required placing the wave packet far from the potential and truncating the

effective potential at a point when it was relatively small compared to other energy scales in the problem. This preserves the approximation of the Møller states as Gaussian potentials.

1.4 Scope and Limitations of Research

The work performed assumes the potentials for the system are known. These potentials are assumed to be symmetric central potentials, with the potentials passed as input to the system. Minimal effort was expended in understanding how the parameters for the potentials are obtained for a specific system. Furthermore, it is assumed that only 2 states influence the collisional transition process.

Initially, line broadening was also to be investigated using the Channel Packet Method and a review paper [3], but this was abandoned due to lack of time. A study of line broadening using the Channel Packet Method could be beneficial to DPAL work and the general spectroscopy community.

1.5 Significance of Research

Often, one reaches a point where several atoms or molecules appear to be suitable for a given purpose, and it is desirable to know in advance which atom or molecule would be best suited for the task at hand.

In DPALs, one of several factors to consider when selecting an alkali is maximizing the ${}^2P_{3/2} \rightarrow {}^2P_{1/2}$ cross section in order to more easily obtain a population inversion in the ${}^2P_{1/2}$ state [14]. It is hoped that a more rigorous understanding of the methods for computing collisional cross sections for this state transition could better model this essential collisional dynamic.

Other applications involving collisional cross sections arise in the realms of chemical physics and spectroscopy, where collisions play a significant role.

II. Gaussian Wave Packet Propagation

Scattering theory describes the interaction of an incoming wave packet with a potential over a certain time. Therefore, any complete discussion of scattering must begin with a discussion of propagating a wave packet through an arbitrary potential. For sake of convenience, the wave packets used as input for this thesis are Gaussian, but this discussion is kept generic to any wave function and any potential.

2.1 Theory of Wave Packet Propagation

Central to any time evolution problem in quantum mechanics is the time evolution operator, the Hamiltonian $\hat{H}$:

$$\hat{H} = \hat{T} + \hat{V} \tag{3}$$

$\hat{T}$ is the kinetic energy and $\hat{V}$ is the potential energy. In matrix mechanics, the Schrödinger equation is as follows:

$$\hat{H}|\psi\rangle = E|\psi\rangle \tag{4}$$

This equation has the following solution if the Hamiltonian is time-independent:

$$|\psi(t)\rangle = e^{-i\hat{H}t/\hbar}|\psi(0)\rangle = e^{-i(\hat{T}+\hat{V})t/\hbar}|\psi(0)\rangle \tag{5}$$

In the coordinate representation, this equation has the following form:

$$\langle x|\psi(t)\rangle = \psi(x,t) = \langle x|e^{-i(\hat{T}+\hat{V})t/\hbar}|\psi(0)\rangle \tag{6}$$

Now, a problem is reached. $\hat{T} + \hat{V}$ is not generally diagonal in the position basis. Furthermore, since $\hat{T}$ and $\hat{V}$ do not necessarily commute, the naïve approximation

below is only accurate to $O(t)$:

$$e^{-i(\hat{T}+\hat{V})t/\hbar} \approx e^{-i\hat{T}t/\hbar}e^{-i\hat{V}t/\hbar} \tag{7}$$

A much better approximation to make will be discussed later, but it is not central to the discussion at present; in order to more clearly illustrate other features of the problem, I will use this approximation and later discuss how to make a more robust approximation. This approximation has only solved half of the problem. Although it is true that $\hat{V}$ is usually diagonal in position space, $\hat{T}$ is not. Fortunately, there is an easy way around this problem. The kinetic energy of a particle is as follows:

$$\hat{T} = \frac{\hat{p}^2}{2m} = \frac{\hbar^2\hat{k}^2}{2m} \tag{8}$$

This means $\hat{T}$ is diagonal in the momentum (p) representation, or analogously, in k-space. If the potential is taken to be diagonal in the position representation (e.g., $V(x)$ is specified), and if the transform from the x representation to the k representation is known, then the problem will be solved. By inserting completeness in the form of $|x\rangle\langle x|$, one can see the transformation of ψ from position space to k-space is simply the Fourier transform [8][7]:

$$\psi(k) = \langle k|\psi\rangle = \int \langle k|x\rangle\langle x|\psi\rangle\, dx = \frac{1}{\sqrt{2\pi}}\int e^{-ikx}\psi(x)\, dx = \mathcal{F}(\psi(x)) \tag{9}$$

The transformation of ψ from k-space to position space is derived analogously, and is the inverse Fourier transform $\mathcal{F}^{-1}$. This differs from the Fourier Transform $\mathcal{F}$ only by replacing the term of e^{-ikx} under the integral with the term e^{ikx}. Therefore, we now have a mechanism to evaluate Equation (6) through the use of completeness over k and x twice each:

$$\langle x|\psi(t)\rangle = \langle x| \int\int\int\int |k\rangle\langle k|e^{-i\hat{T}t/\hbar}|k'\rangle\langle k'|x'\rangle\langle x'|e^{-i\hat{V}t/\hbar}|x''\rangle\langle x''|\psi(0)\rangle \, dk \, dk' \, dx' \, dx''$$

$$= \int\int\int\int \langle x|k\rangle e^{-iT(k)t/\hbar}\langle k|k'\rangle\langle k'|x'\rangle e^{-iV(x'')t/\hbar}\langle x'|x''\rangle\langle x''|\psi(0)\rangle \, dk \, dk' \, dx' \, dx''$$

$$= \int\int \langle x|k\rangle e^{-iT(k)t/\hbar}\langle k|x'\rangle e^{-iV(x')t/\hbar}\langle x'|\psi(0)\rangle \, dk \, dx'$$

$$= \mathcal{F}^{-1}\left[e^{-iT(k)t/\hbar}\mathcal{F}(e^{-iV(x)t/\hbar}\langle x|\psi(0)\rangle)\right] \tag{10}$$

2.1.1 Split Operator Method.

As pointed out previously, it is necessary to make an approximation to $e^{-i(\hat{T}+\hat{V})t/\hbar}$ as well for a general potential. Up to this point, we have used the approximation in Equation (7) for simplicity, despite its numerical instability. It is now time to fix that simplification. A much better approximation is as follows:

$$e^{-i(\hat{T}+\hat{V})t/\hbar} \approx e^{-i\hat{V}t/(2\hbar)}e^{-i\hat{T}t/\hbar}e^{-i\hat{V}t/(2\hbar)} \tag{11}$$

This is known as the Split Operator method [4], which is widely used for Time-Dependent problems because of its increased numerical stability at relatively low cost. As a result, Equation (5) is rewritten as:

$$e^{-i(\hat{T}+\hat{V})t/\hbar}|\psi(0)\rangle \approx e^{-i\hat{V}t/(2\hbar)}e^{-i\hat{T}t/\hbar}e^{-i\hat{V}t/(2\hbar)}|\psi(0)\rangle \tag{12}$$

It can be shown that the equation is approximately true to $O(t^2)$ (that is, the error term scales as t^2) by simply taking a Taylor expansion of both sides of the equation and comparing powers of t, taking care to consider $\hat{T}$ and $\hat{V}$ do not, in general, commute. This introduces an algorithmic error of $O(t^3)$. This modification also does not fundamentally alter the development undertaken in the previous section. It does

add another elementwise multiply (which takes time $O(N)$) by modifying Equation (10) to become:

$$\psi(x,t) = e^{-iV(x)t/(2\hbar)}\mathcal{F}^{-1}\left\{e^{-iT(k)t/\hbar}\mathcal{F}\left[e^{-iV(x)t/(2\hbar)}\psi(x,0)\right]\right\} \tag{13}$$

Since the FFT routine is $O(N\,log_2\,N)$, adding an $O(N)$ operation does not significantly alter runtime, and the added numerical stability ensures rapid convergence, so the use of this approximation instead of the more straightforward Equation (10) is justified.

2.1.2 Absorbing Boundary Conditions.

For potentials of interest, it may be necessary to propagate the wave packet over long time scales in order to fully pass through the potential. Through standard propagation techniques, this would require a large enough grid in position space to hold the entire packet through the calculation. However, it will be shown in Chapter III, Equation (25), that the wave packet information is no longer required once it has propagated through the potential and beyond a certain point.

For this reason, without any loss of information, it is possible to prematurely truncate the grid in position space by utilizing absorbing boundary conditions. The simplest way to do this is by adding an absorbing potential, such that the potential is of this form:

$$V(x) = \begin{cases} V_0(x) + iV_{abs}(x) & \text{for } x \geq 0 \\ V_0(x) - iV_{abs}(x) & \text{for } x < 0 \end{cases} \tag{14}$$

A natural choice of the absorbing potential is a Gaussian. It is possible for this effective potential to cause reflections. These reflections may be minimized by choosing a relatively broad Gaussian in position space. The effect of this absorbing potential is

to rapidly reduce the value of the wave packet at the boundary, as shown by Equation (13).

2.1.3 3-D Spherical Central Potentials.

When propagating through a spherically symmetric central potential and solving Schroedinger's Equation, one can assume the following form for the solution (where $\mathbf{r}$ is a 3-D vector and r, θ, ϕ are the three scalar components of that vector):

$$\psi_{n,l,m}(\mathbf{r}) = R_{n,l}(r)Y_l^m(\theta,\phi) = \frac{1}{r}u_{n,l}(r)Y_l^m(\theta,\phi) \tag{15}$$

The $Y_l^m(\theta,\phi)$ function is known, and therefore, the problem has been reduced from three dimensions to one dimension, determining the value of $u_{n,l}(r)$. Any spherically symmetric central potential may be reduced in this manner. The solution for $u_{n,l}(r)$ may be obtained by plugging the assumed form above into the Schroedinger equation, obtaining [7]:

$$\left[-\frac{\hbar^2}{2m}\frac{d^2}{dr^2} + \frac{l(l+1)\hbar^2}{2mr^2} + V(r)\right]u_{n,l}(r) = \frac{\hbar^2k^2}{2m}u_{k,l}(r) \tag{16}$$

The potential $V(r)$ must decay faster than $1/r$ for this method to succeed. This means the Coulomb potential may not be analyzed using this split operator method in a single dimension.

2.2 Initial Wave Packet

There is a remaining issue with wave packet propagation yet to be discussed. What is $|\psi(x,0)\rangle$? In this thesis, Gaussian wave packets will be used, with the following form:

$$\psi(x) = \left(\frac{1}{2\pi(\Delta x_0)^2}\right)^{1/4} \times exp\left[\frac{-(x-x_0)^2}{4(\Delta x_0)^2} + ik_0(x-x_0)\right] \tag{17}$$

The parameters of the Gaussian wave packet are as follows:

- x_0 is the location of the peak in position space
- Δx_0 is the width
- k_0 is the location of the peak momentum in k-space
- m is the mass

The width of the Gaussian in k-space at $t = 0$ is such that $\Delta x \Delta k = 1/2$, the minimum uncertainty, as can be obtained analytically from the Fourier transform of the above equation:

$$\psi(k) = \left(\frac{2(\Delta x_0)^2}{\pi}\right)^{1/4} exp\left[-[\Delta x_0(k-k_0)]^2 - ikx_0\right] \tag{18}$$

There is flexibility in the choice of these parameters for the Gaussian. (In fact, the Gaussian shape is not special; any initial wave packet can be chosen, so long as it meets a few relatively lenient constraints described in Chapter III.) In the Chapter IV, we will see that judicious choice of these parameters can ensure the most relevant collisional information is extracted. Although this choice of $|\psi\rangle$ appears arbitrary at present, it is because the scattering operator is independent of $|\psi\rangle$, as will be shown in Chapter III.

III. One Dimensional Collisional Transitions

3.1 Overview

Now that an arbitrary wave packet may be propagated through an arbitrary potential, the next step is to use the propagation information to extract collisional data. Let $\hat{S}$ be an operator such that:

$$|\psi_f\rangle = \hat{S}|\psi_i\rangle \tag{19}$$

Here, $|\psi_f\rangle$ is the final (product) wave packet and $|\psi_i\rangle$ is the initial wave packet. $\hat{S}$ is known to be time-independent. The operator is also clearly unitary and Hermitian. The question of collisions then is reduced to a question of what the operator $\hat{S}$ consists of for a given system.

The S-matrix is defined as $\langle k'|\hat{S}|k\rangle$[6], or the representation of the operator $\hat{S}$ in k-space. For propagation through free space ($\hat{V} = 0$), it is obvious that no collision can possibly occur. This means $\hat{S} = \hat{1}$, and $k' = k$ for nonzero entries in the S-matrix. Propagation through an arbitrary potential can lead to one or more of the following for different energies, and thus different values of k:

- Transmission ($k' = k$)
- Reflection ($k' = -k$)
- Energy Transfer ($|k'| \neq |k|$)

Energy transfer can only occur in an inelastic collision, by definition. Although inelastic scattering is at the heart of this thesis, it is important to first describe elastic scattering, both as a test to ensure functional code and as a precursor for the more complex case of scattering through an arbitrary potential.

3.2 Elastic Scattering

Consider elastic scattering by a particle with energy E. Since the spherical potential has been reduced to one dimension, there are only two possible resulting values of k in the asymptotic limit, as follows:

$$\pm k = \pm \frac{\sqrt{2mE}}{\hbar} \tag{20}$$

Since there are only two possible values of k, the complete S-matrix for a single initial energy E may be represented by a 2x2 matrix. For each energy, the S-matrix is represented as a 2x2 matrix as follows:

$$\mathbb{S} = \begin{bmatrix} S_{++} & S_{+-} \\ S_{-+} & S_{--} \end{bmatrix} \tag{21}$$

The sign represents whether the k-value is $+|k|$ or $-|k|$. The first sign is the product (output) k-value, and the second sign is the reactant (input) k-value; for example, $S_{+-} = \langle +k|\hat{S}| - k\rangle$. Clearly, transmission is represented by the diagonal elements of this 2x2 matrix, and reflection is represented by the off-diagonal elements. Since the collision is elastic, all other matrix elements corresponding to different k-values (and therefore different energies) must be 0, by definition. Therefore, this 2x2 matrix must be unitary. The only remaining step is to find the actual S-matrix entries, which will be discussed in section 3.5.

For a spherically symmetric central potential, this matrix may be further simplified. If the packet begins in the asymptotic limit at large r, then a packet with initial momentum $+\hbar k$ does not undergo a collisional transition, so that matrix element must be 0. Furthermore, a packet with final momentum in the asymptotic limit of $-\hbar k$ has not yet undergone a collision, and thus is not the final momentum, so

that matrix element also must be 0. This means only the matrix element S_{+-} has a nonzero entry for a spherically symmetric central potential.

3.3 Inelastic Scattering

In the case of inelastic scattering, for a given initial energy E, there are still only two possible input k values, $+k$ and $-k$, but there are now an infinite number of possible output k values, in general, corresponding to a different product energy E_f.

Fortunately, in quantum mechanical transitions, we are often interested only in transitions between a relatively small number of total states. In this thesis, we will assume the two-state approximation holds. Therefore, there are only a total of 2 possible final energies, and therefore 4 possible final k-values, corresponding to non-zero elements of the S-matrix.

This leads to the following general form for the S-matrix for a given input energy E:

$$\begin{bmatrix} S_{+k1,+k1} & S_{+k1,-k1} & S_{+k1,+k2} & S_{+k1,-k2} \\ S_{-k1,+k1} & S_{-k1,-k1} & S_{-k1,+k2} & S_{-k1,-k2} \\ S_{+k2,+k1} & S_{+k2,-k1} & S_{+k2,+k2} & S_{+k2,-k2} \\ S_{-k2,+k1} & S_{-k2,-k1} & S_{-k2,+k2} & S_{-k2,-k2} \end{bmatrix}$$

As in the elastic scattering case, this matrix must be unitary in the two-state approximation. The upper half of the matrix corresponds to the elastic scattering case, and the lower half of the matrix corresponds to the inelastic scattering case, so this matrix may be written simply as:

$$\begin{bmatrix} \mathbf{S_{k1\to k1}} & \mathbf{S_{k2\to k1}} \\ \mathbf{S_{k1\to k2}} & \mathbf{S_{k2\to k2}} \end{bmatrix}$$

Obviously, the diagonal entries of this supermatrix are the elastic scattering and the off-diagonal elements are inelastic scattering.

This may be further simplified for spherically symmetric central potentials, using the same logic as in the preceding section. Under a spherically symmetric potential in the asymptotic limit, $k_1 < 0$ (the initial Møller packet is propagating into the potential from the asymptotic limit) and $k_2 > 0$ (the final Møller packet has completely reflected off the potential).

Therefore, the nonzero elements of the S-matrix for spherically symmetric central potentials when beginning in the asymptotic limit are simply:

$$\begin{bmatrix} S_{+k1,-k1} \\ S_{+k2,-k1} \end{bmatrix}$$

For a spherically symmetric central potential, the following property must therefore be true since the S-matrix is unitary:

$$|S_{+k2,-k1}|^2 + |S_{+k1,-k1}|^2 = |S_{elastic}|^2 + |S_{inelastic}|^2 = 1 \tag{22}$$

($S_{elastic} = S_{+k1,-k1}$ and $S_{inelastic} = S_{+k2,-k1}$). This important result for a spherically symmetric potential in the 2-state approximation may at first seem trivial, but it gives an important mechanism to determine the error in the method if both the elastic and inelastic scattering results are calculated.

3.4 Interpretation of S-matrix

Each element of the S-matrix is defined as follows [6]:

$$S^l_{kf,ki} = A_l e^{2i\delta_l} \tag{23}$$

Here, δ_l is a real number, and A_l is an amplitude less than or equal to 1. If all of the packet transitions from k_i to k_f, the amplitude A_l must be 1, since the S-matrix is unitary. As the magnitude decreases, the probability amplitude of transitioning to $+k_f$ decreases. For the special case of a spherically symmetric potential ($k_i < 0$ and $k_f > 0$), if $|k_i| = |k_f|$ (elastic scattering), the magnitude A_l is directly proportional to the degree of inelasticity of the transition. If the transition is completely elastic, $A_l = 1$; if the transition is completely inelastic, $A_l = 0$. Each S-matrix element can be thought of as describing the rotation of an incoming wave by an angle δ_l relative to propagation through free space.

More precisely, assume propagation of a wave through no potential ($\hat{V} = 0$). There will be no scattering, and therefore the S-matrix should be purely diagonal, but it is still not precisely defined because it may differ by an overall global phase. Let $\delta_l = 0$ in this case be the reference for the angle to define the global phase factor. For an arbitrary reflective potential, the scattering rotation is given by δ_l. The factor of 2 simply takes into account a particle's reflection. The particle traverses the same distance in space twice, once as an incoming wave and once as a reflected wave.

There are other definitions of the global phase, resulting in other matrices, such as the T-matrix and K-matrix. These matrices are all related to one another, and provide no additional fundamental information [6]. Therefore, the S-matrix is used throughout this thesis.

3.5 Channel Packet Method

Several methods have been devised to calculate S-matrix elements. In this thesis, a method devised by David J. Tannor and David E. Weeks in 1993 [18] called the Channel Packet Method is used. This method may be outlined as follows:

- Choose an initial wave packet entirely in either $+k$ or $-k$ space, and located

anywhere in position space

- Propagate the initial wave packet under the Møller initial operator to obtain the Møller initial state
- Choose a final wave packet state entirely in either $+k$ or $-k$ space, and located anywhere in position space
- Propagate the final wave packet under the Møller final operator to obtain the Møller final state

Propagate the Møller initial state forward in time under the full Hamiltonian:

- Propagate by Δt using the method described in Chapter II
- Build the correlation function by recording the projection on to the Møller final state as a function of time

Terminate propagation when future contribution to correlation function is negligible

- Take the Fourier transform of the correlation function in energy space
- Compute the S-matrix element for each value of interest using Equation (25)

The Møller initial (+) and final (-) operators are defined as follows (where $\hat{H}_0$ is the asymptotic Hamiltonian, and $\hat{H}$ is the full Hamiltonian):

$$\hat{\Omega}_{\pm} = \lim_{t \to \infty} e^{\mp i\hat{H}t} e^{\pm i\hat{H}_0 t} \tag{24}$$

Physically, the Møller initial (final) operator propagates a wave packet backward (forward) in time under the asymptotic Hamiltonian, then forward (backward) in time to time $t = 0$ under the full Hamiltonian. If the wave packet is entirely contained in the asymptotic Hamiltonian, there is no net effect.

Table 2. Expansion coefficients to determine S-matrix elements

	$S_{+k,+k}$	$S_{+k,-k}$	$S_{-k,+k}$	$S_{-k,-k}$
$\eta_+(k) = 0$ for:	$k < 0$	$k > 0$	$k < 0$	$k > 0$
$\eta_-(k) = 0$ for:	$k < 0$	$k < 0$	$k > 0$	$k > 0$

It is important to eliminate any influence of the initial wave packet choice on the observed S-matrix elements. Therefore, to compute the S-matrix elements at each k-value, it is necessary to normalize by the following equation:

$$\langle k_f|\hat{S}|k_i\rangle = S_{k_f,k_i} = \frac{\hbar|k|\langle\psi_-|A_E^+\rangle}{2\pi m\eta_-^*(k_f)\eta_+(k_i)} \tag{25}$$

In this equation, ψ_- is the Møller final state and ψ_+ is the Møller initial state. η_- is the expansion coefficient of ψ_-, and η_+ is similarly the expansion coefficient of ψ_+. $\langle\psi_-|A_E^+\rangle$ is the Fourier transform of the correlation function:

$$\langle\psi_-|A_E^+\rangle = \int e^{iEt}\langle\psi_-|e^{-i\hat{H}t}|\psi_+\rangle\, dt \tag{26}$$

The energy E is the total asymptotic energy, including both potential energy and kinetic energy. It is calculating $\langle\psi_-|A_E^+\rangle$ that is the essential component of Equation (25) in the Channel Packet Method; the rest of the equation is just normalization. In order to more fully understand this quantity, Equation (26) may be rewritten as [18][21] [22]: (here, * means complex conjugate)

$$\begin{aligned}\langle\psi_-|A_E^+\rangle = \frac{2\pi m}{|k|}[&\eta_-^*(-k)\eta_+(+k)S_{-k,+k} + \eta_-^*(+k)\eta_+(+k)S_{+k,+k} + \\ &\eta_-^*(-k)\eta_+(-k)S_{-k,-k} + \eta_-^*(+k)\eta_+(-k)S_{+k,-k}]\end{aligned} \tag{27}$$

Therefore, at first glance it appears possible to obtain a superposition of S-matrix elements using this method. Actually, the $\eta_\pm(\pm k)$ are expansion coefficients that are

chosen by the initial wave packet. By judicious choice of the Møller initial and final states, it is possible to obtain a particular S-matrix element. In fact, since the initial and final Møller states are spread in k-space, it is possible to obtain a small number of S-matrix elements using this technique. Table 2 summarizes the appropriate choices for the Møller initial and final states in order to calculate the desired type of S-matrix elements.

3.6 Diabatic, Adiabatic, and Coupling Potentials

In many instances, inelastic scattering is of interest. The simplest approach to modeling inelastic collisions in quantum mechanics is to assume only two states are involved in the collision. All other contributions are assumed negligible.

In the two-state approximation, the Hamiltonian is now a 2x2 matrix at each point in either position or momentum space. Unfortunately, the Hamiltonian for a general system is not diagonal in both position space and momentum space through only the Fourier transform. This is due to an interaction term which models the off-diagonal probability amplitude of transitioning from state 2 to state 1 (or vice versa). This amplitude is assumed to be real, and is known as the coupling potential. The potentials which diagonalize the Hamiltonian in momentum space are known as the diabatic potentials, while the potentials which diagonalize the Hamiltonian in position space are known as the adiabatic potentials.

Through straightforward linear algebra techniques, it is possible to obtain the adiabatic potentials from the diabatic potentials and the coupling potential by obtaining the eigenvalues and eigenvectors of a 2x2 matrix at each point in space. That is, for a given point in space, the diabatic potential takes the following form [4]:

$$\begin{bmatrix} V_{11}(r) & V_{12}(r) \\ V_{12}(r) & V_{22}(r) \end{bmatrix}$$

This matrix is symmetric and real, and therefore the eigenvectors simply form a rotation matrix.

The Channel Packet Method is unchanged by the two-state approximation, other than tracking on which of the two potential surfaces the Møller initial and final states are located. However, when propagating the wave packet, exponentiating an operator makes sense only in the diagonal representation of that operator. Therefore, it is necessary to convert from the diabatic to the adiabatic representation prior to applying the potential energy operator $\hat{V}$, and it is necessary to convert from the adiabatic representation to the diabatic representation prior to applying the kinetic energy operator $\hat{T}$ [4]. This ensures the operators $\hat{T}$ and $\hat{V}$, which are now 2x2 matrices at each point in space, are diagonal prior to exponentiation.

Since both the adiabatic and diabatic representations are required to perform the wave packet propagation, it is natural to ask what minimum amount of information is sufficient in order to obtain both the adiabatic and diabatic representations. Any one of the following triplets of information is sufficient in order to obtain the full diabatic and adiabatic potentials:

- Both diabatic potentials and the coupling potential
- Both adiabatic potentials and the coupling potential
- Both adiabatic potentials and the rotation angle as a function of position

For a more detailed discussion of how to convert between diabatic and adiabatic representations, to include a procedure to estimate the diabatic potentials from the

adiabatic potentials and the crossing point, the reader is referred to Faist, Levine, and Bernstein [10][11].

3.7 Determination of Scattering Cross-Sections

Scattering cross sections are a direct result of collisional interactions.

As discussed in Chapter II, the 3-D spherically symmetric central potential problem may be reduced to one dimension. From Equation (16), the angular dependence can be captured by introducing an effective potential term [6][7]:

$$V_{eff}(r) = V(r) + \frac{l(l+1)\hbar^2}{2mr^2} \tag{28}$$

The elastic, collisional (absorption), and total cross-sections for a spherically symmetric potential (where $k_i < 0$ and $k_f > 0$ are the only nonzero entries) are calculated as follows [7]:

$$\sigma_{i\to i} = \sigma_{el} = \frac{\pi}{k^2}\sum_{l=0}^{\infty}(2l+1)|1 - S_{i,i}^l|^2 \tag{29}$$

$$\sigma_{i\to f} = \sigma_{coll} = \frac{\pi}{k^2}\sum_{l=0}^{\infty}(2l+1)|S_{f,i}^l|^2 \tag{30}$$

$$\sigma_{tot} = \sum_j \sigma_{i\to j} = \frac{2\pi}{k^2}\sum_{l=0}^{\infty}(2l+1)(1 - \Re(S_{i,i}^l)) \tag{31}$$

In these equations, it is assumed that i, f, and j are state labels, and that $f \neq i$. For the total cross section, the summation is over both $j = i$ (elastic) and $j \neq i$ (inelastic) cross sections.

Calculation of $\sigma_{i\to f}$ $(f \neq i)$ is the primary goal of this thesis. Theoretically, σ_{tot} could be calculated independently to determine an error estimate for $\sigma_{i\to f}$, but in

practice, it was found that σ_{el} (and therefore σ_{tot}) required a summation over a larger range of l values, and therefore, this approach was not used as an error estimate. Further details are discussed in Chapters IV and V.

3.8 Transition Rates and Cross Sections

The scattering cross sections in Equations (29-31) assume only a single energy is present in the system. In experimental measurements, there is some distribution of energies (generally assumed to be a Boltzmann distribution). Therefore, the results from the Method of Partial Waves must be convolved with a Boltzmann disbribution centered at the desired temperature of interest to account for the statistical mechanics of the system.

Fortunately, using the Channel Packet Method, the S-matrix element for a wide range of energies may be calculated simultaneously. The data presented in this thesis is the raw distribution from the Method of Partial Waves, prior to convolution with a distribution function.

This thesis is primarily concerned with calculation of cross sections, from which the transition rate may be obtained [9].

IV. Numeric Considerations

4.1 Overview

The sequential procedure employed in this thesis for calculating a cross section is as follows:

- Determine the range of energies to obtain cross section information across
- Determine the Hamiltonian, wave packet, and base propagation parameters
- Determine r_{max} and k_{max} from these inputs and a tolerable minimum level of error
- Determine l_{max} using Equation (36)

  For each l value from 0 to l_{max}:

- Propagate the wave packet through this effective potential and obtain the scattering matrix elements using the procedure described in Chapter II

  For each k-value that contains numerically stable information:

- Combine all scattering matrix elements to obtain $\sigma_{i\rightarrow f}$ using Equation (30)

  Continue the above process until $\sigma_{i\rightarrow f}$ has converged over the range of energies of interest.

The remainder of this chapter focuses on numerical pitfalls and suggestions to optimize parameter choice, as well as a few suggestions on how to perform error analysis.

4.2 General Guidelines on Input Parameters

To obtain an experimentally observed cross section, it is necessary to obtain several different absorption cross sections and convolve the results with the Boltzmann distribution. Using the Channel Packet Method, it is possible even in the presence of numerical error to calculate many cross sections from a single set of propagation values, provided all of the k-values are sufficiently close to the initial maximum k-value to minimize numerical error in the calculation of the S-matrix elements.

Recall that $\Delta x \Delta k = 1/2$ (atomic units) for our chosen Gaussian at $t = 0$. It is therefore desirable for Δk to be as large as possible, and thus Δx as small as possible, within the following limits:

- The initial k values of the wave packet and the k of the Møller packet must either be all positive or all negative (to within an acceptable degree of error), although the wave packet may be all $-k$ and the Møller final packet all $-k$, or vice versa.

- Smaller Δx means a larger number of sampling points is required to minimize propagation error and obtain an accurate value for the projection onto the Møller final packet.

A good rough rule of thumb is the resulting scattering data will be valid in the range $k_0 \pm 3\Delta k$. This is merely a rough gideline for setting parameter information at the start, and is not guaranteed. It is based only on my experience in analyzing scattering data in the absence of significant propagation errors, although there are several factors which may cause the actual performance to be worse (or better).

The sections that follow contain analysis to ensure the code is functional.

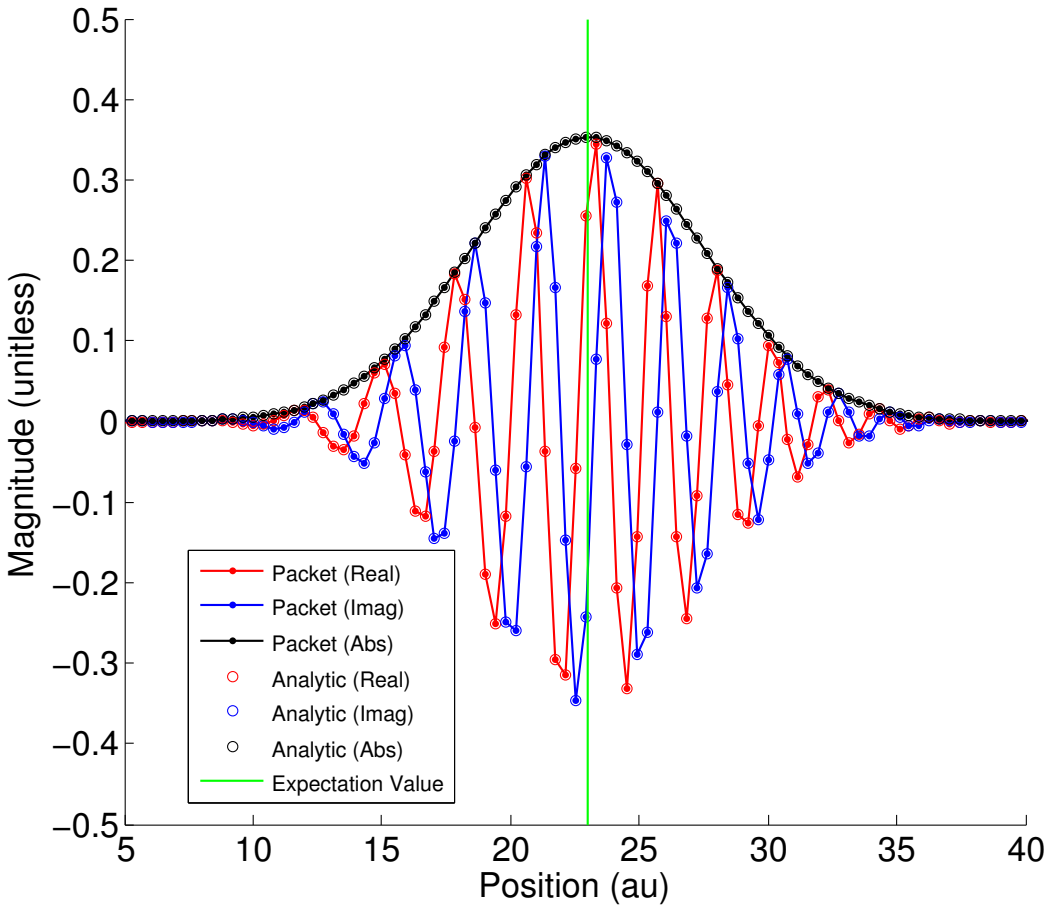

Figure 1. Gaussian wave packet propagated through 100 time steps and compared to the analytic solution for a free particle.

4.3 Propagation

To verify the propagator code developed operates correctly, two test potentials were used where the analytic solutions are known in each case. Propagation through free space ($\hat{V} = 0$) is the simplest case of wave packet propagation, and propagation in the ground state of a harmonic oscillator ($\hat{V} = 1/2m\omega^2\hat{x}^2$) results in a coherent state.

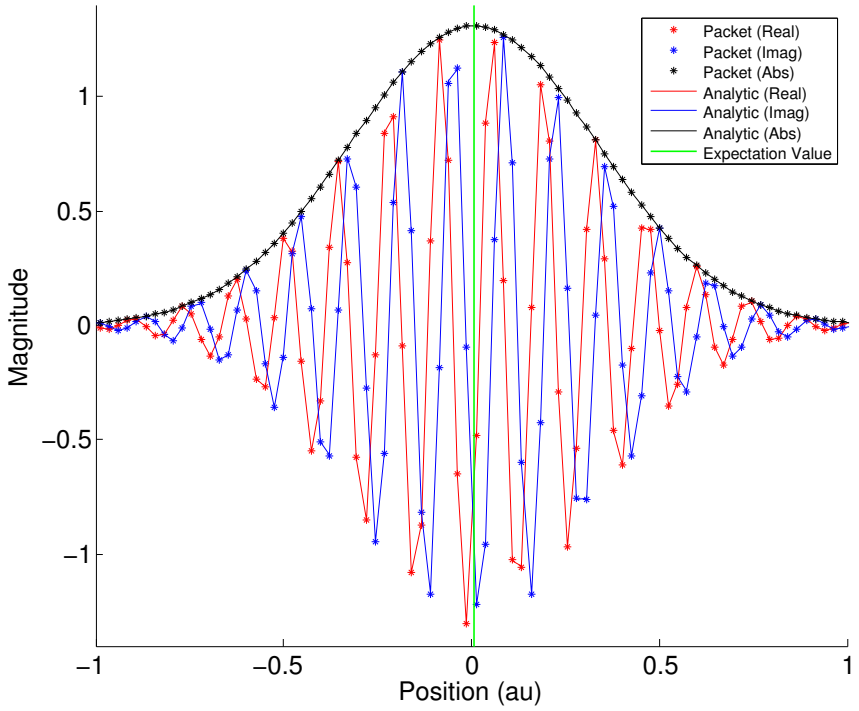

Figure 2. Wave packet for diatomic Hydrogen propagated to a time of 1728 au in a harmonic oscillator as a coherent state and compared to analytic solution

4.3.1 Free Space Propagation.

In free space ($\hat{V} = 0$), the time evolution of the initial Gaussian wave packet given by equation 17 may be determined analytically as follows:

$$\psi(x,t) = \left(\frac{1}{2\pi(\Delta x_0)^2}\right)^{1/4}\left(1+\frac{i\hbar t}{2(\Delta x_0)^2 m}\right)^{-1/2}\times$$
$$exp\left[\frac{-\frac{(x-x_0)^2}{4(\Delta x_0)^2}+ik_0(x-x_0)-ik_0^2\frac{\hbar t}{2m}}{1+\frac{i\hbar t}{2(\Delta x_0)^2 m}}\right] \tag{32}$$

A wave packet was propagated through 100 iterations and compared to this analytic result. Results are shown in Figure (1).

4.3.2 Coherent State Propagation.

To verify the propagation code worked with a potential applied, it was tested against a coherent state. A coherent state is a state in which the exectation value is identical to the classical expectation value with time, both for the position and the momentum, and the magnitude remains constant with time – the wave packet does not spread [8]. This makes a very convenient test case, since several quantum mechanical properties can now be compared to their classical analogue, and an analytic form may be specified.

To perform this test, the following parameters were used:

```
------------------------------------------------------------------------
Initial Gaussian Wave Packet Parameters
------------------------------------------------------------------------
x0 = 5.0000000E+000    k0 = 0.0000000E+000    dx0 = 2.3338001E-001
m = 9.1800000E+002
<x> = 5.0000000E+000
------------------------------------------------------------------------
Hamiltonian Parameters
------------------------------------------------------------------------
Kinetic: Normal
Potential: Simple Harmonic Oscillator
m = 9.1800000E+002    w = 1.0000000E-002    x0 = 0.0000000E+000
Angular Momentum: l =  0
Boundary Conditions: None
------------------------------------------------------------------------
Propagation Parameters
------------------------------------------------------------------------
x =-1.0000000E+002 to 1.0000000E+002; dx = 2.4417043E-002 (N = 8192)
k =-1.2863252E+002 to 1.2866393E+002; dk = 3.1412092E-002
t = 0.0000000E+000 to 2.0000000E+003; dt = 1.0000000E+000
(iterations: 2000)
------------------------------------------------------------------------
```

`N` is the number of points in the discretization. All values are in atomic units.

This wave packet was propagated through time and compared to the analytic solution at a few data points. The results are plotted in Figure 2, where it is clear

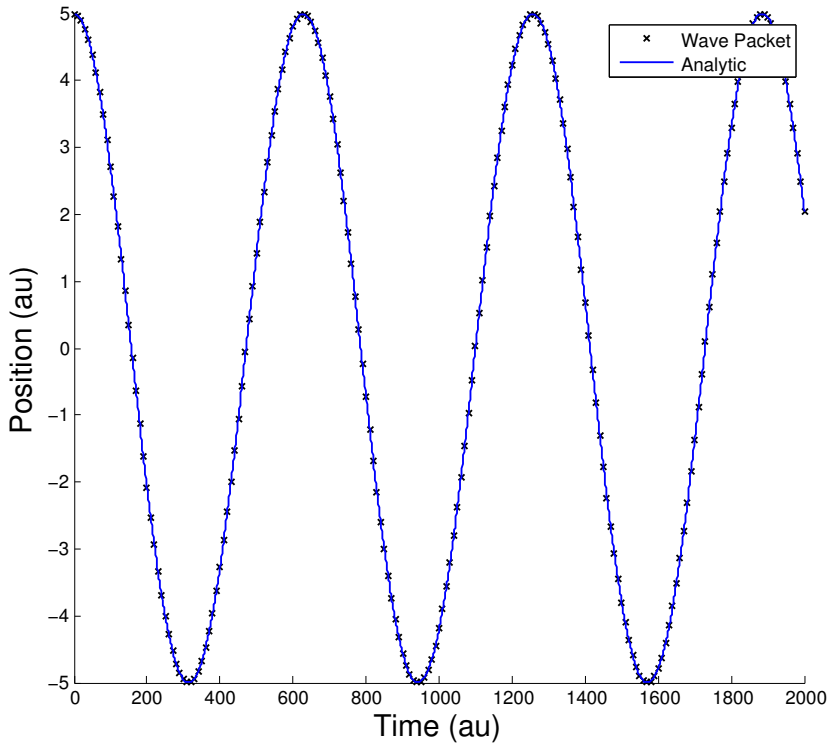

Figure 3. Expectation value of position of wave packet every 10 au for diatomic Hydrogen in a harmonic oscillator as a coherent state and compared to analytic solution

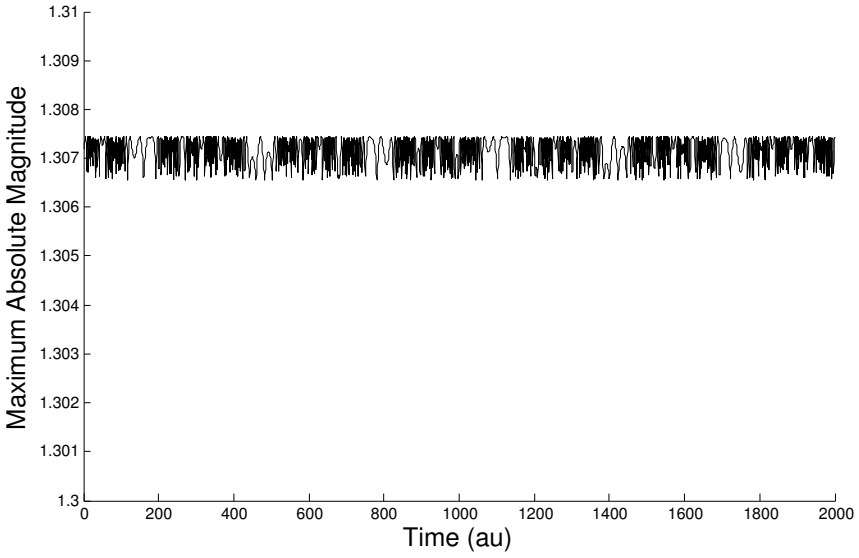

Figure 4. Maximum magnitude of wave packet for diatomic Hydrogen in a harmonic oscillator as a coherent state. The value remains relatively constant around 1.307.

the analytic and computed points match up precisely. The expectation value of the position is also examined as a function of time and plotted in Figure 3. The expectation value fits to $y = 5\,cos(0.01t)$, as expected from the inputs, with an RMS error of 4.206×10^{-10}. Finally, for a coherent state, the packet should have no spread in time. Since $\langle\psi|\psi\rangle = 1$ and the wave packet maintains a Gaussian shape, it is sufficient to examine the maximum value of the magnitude of the wave function as a function of time to ensure it remains constant. These results are plotted in Figure 4. All of these tests performed as expected, indicating the propagation code worked properly.

4.4 Scattering Calculations

To verify the calculation of scattering matrix elements after propagation, there are two approaches that may be used. The first approach is to simply propagate a wave packet through no potential and calculate the S-matrix elements, which should all be 1, since the S-matrix global phase factor is defined by this value. The second method is to propagate a wave packet through a square potential *without absorbing boundary conditions* until the packet has propagated completely through the potential and ensuring the square of the S-matrix elements match with the ratio of transmitted packet to initial packet, and reflected packet to initial packet. Since the propagator code was verified in the previous section using a separate technique, this shows the scattering calculations are performed correctly.

4.4.1 "Scattering" through free space.

The following parameters were used to calculate the scattering matrix elements through free space:

```
Initial Gaussian Wave Packet Parameters
-----------------------------------------------------------------
x0 = 9.0000000E+001    k0 = 8.0000000E+000    dx0 = 5.0000000E-001
m = 9.1800000E+002 (atomic units)
<x> = 9.0000000E+001
-----------------------------------------------------------------
Moller Final State Parameters
-----------------------------------------------------------------
x0 = 1.1000000E+002    k0 = 8.0000000E+000    dx0 = 5.0000000E-001
m = 9.1800000E+002 (atomic units)
-----------------------------------------------------------------
Hamiltonian Parameters
-----------------------------------------------------------------
  Kinetic: Normal
Potential: None
Angular Momentum: l =  0
Boundary Conditions: None
-----------------------------------------------------------------
Propagation Parameters
-----------------------------------------------------------------
x = 0.0000000E+000 to 3.0000000E+002; dx = 3.6625565E-002
(N =         8192)
k =-8.5755010E+001 to 8.5775951E+001; dk = 2.0941394E-002
t = 0.0000000E+000 to 8.0000000E+003; dt = 1.0000000E+000
(iterations:     8000)
-----------------------------------------------------------------
```

Clearly in this case the "scattering" is elastic, so $k_i = k_f$. The expected result is for the real part of the scattering matrix element to be 1 and the imaginary part of the scattering matrix element to be 0.

Figure 5 contains the actual results. Since $\Delta x = 0.5$ for this run, $\Delta k = 1$ because $\Delta x \Delta k = 1/2$ for a Gaussian at $t = 0$. The results become less accurate with increasing distance from k_0. Beyond around $4\Delta k$, the data becomes completely unreliable as numerical error due to the small values of the wave packet and finite storage of double-precision numbers overshadow any computation of the actual matrix element.

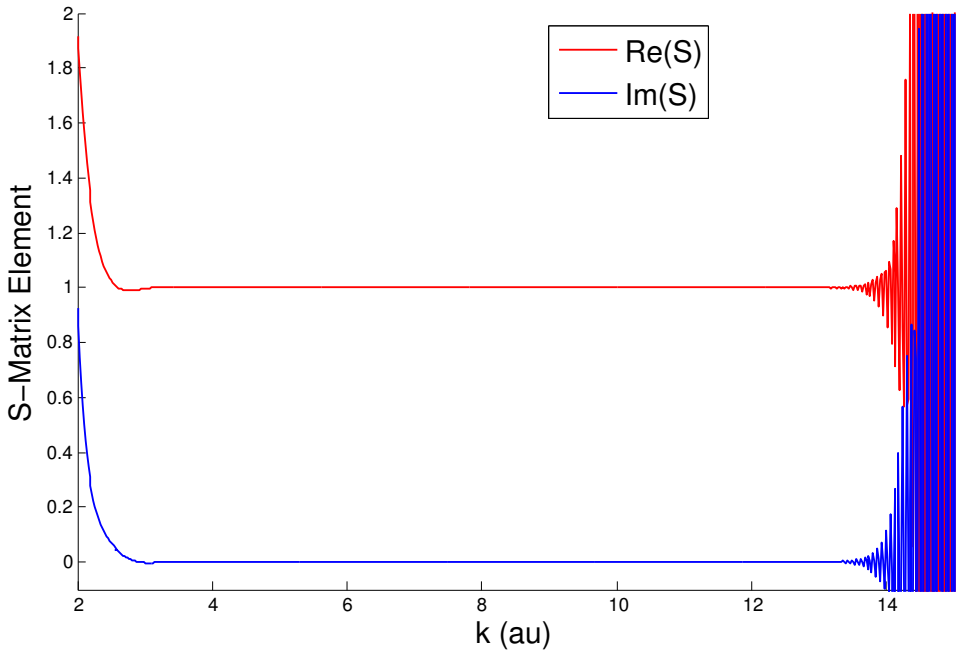

Figure 5. "Scattering" through no potential for a wave packet centered at $k_0 = 8$ with $\Delta k = 1$ ($\Delta x = 0.5$). Only data within about $4\Delta k$ is close to the correct value, with decreasing accuracy with increasing distance from k_0.

4.4.2 Scattering through a Square Potential.

A simple conservation of energy calculation was performed through a square potential to further verify the scattering code. When scattering through a square potential that is 0 on both sides and has a depth $-V_0$, there are two possible results: reflection and transmission.

Assume the initial wave packet $|\psi_0\rangle$ is entirely in $+k$ space, with initial momentum $+k_0$, and completely outside the square potential. Propagate the wave packet through the square potential until it has passed completely through the square potential and is either entirely reflected or entirely transmitted; let this final state be $|\psi_f\rangle$. Calculate the S-matrix elements for transmission (in $+k$ space beyond the square well) and reflection (in $-k$ space before the square well); let S_T and S_R represent these S-matrices. $|S_T(k)|^2 + |S_R(k)|^2 = 1$ for all values of k (there is no other possible state

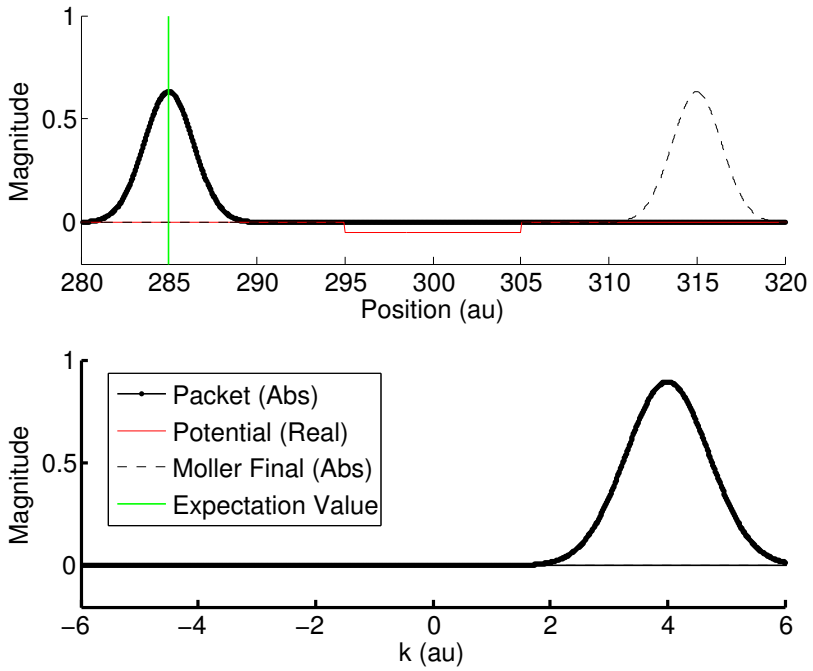

Figure 6. Initial conditions for propagation of wave packet through square potential

for the packet).

Another test may be performed if absorbing boundary conditions are not used. The following equations hold for a square potential [19]:

$$T = \frac{|\langle +k|\psi_f\rangle|^2}{|\langle +k|\psi_0\rangle|^2} \tag{33}$$

$$R = \frac{|\langle -k|\psi_f\rangle|^2}{|\langle +k|\psi_0\rangle|^2} \tag{34}$$

Due to numerical error, it is expected that these equations will hold only for initial k sufficiently close to k_0. To test the scattering code for transmission, the following parameters were used (as illustrated in Figure 6):

```
------------------------------------------------------------------------
Initial Gaussian Wave Packet Parameters
------------------------------------------------------------------------
 x0 = 2.8500000E+002     k0 = 4.0000000E+000     dx0 = 1.0000000E+000
  m = 9.1800000E+002 (atomic units)
```

```
<x> = 2.8500000E+002
------------------------------------------------------------------------
Moller Final State Parameters
------------------------------------------------------------------------
 x0 = 3.1500000E+002    k0 = 4.0000000E+000    dx0 = 1.0000000E+000
  m = 9.1800000E+002 (atomic units)
------------------------------------------------------------------------
Hamiltonian Parameters
------------------------------------------------------------------------
  Kinetic: Normal
Potential: Square Well
xmin = 2.9500000E+002    xmax = 3.0500000E+002    h =-5.0000000E-002
  yl = 0.0000000E+000      yu = 0.0000000E+000
Angular Momentum: l =  0
Boundary Conditions: None
------------------------------------------------------------------------
Propagation Parameters
------------------------------------------------------------------------
x = 0.0000000E+000 to 6.0000000E+002; dx = 3.6623329E-002
(N =        16384)
k =-8.5770716E+001 to 8.5781187E+001; dk = 1.0471336E-002
t = 0.0000000E+000 to 1.5000000E+004; dt = 1.0000000E+000
(iterations:    15000)
------------------------------------------------------------------------
```

A second scattering calculation was performed with identical parameters, except with the Møller final state centered at $x_0 = 280$ and $k_0 = -4$ to detect the reflection from the square potential. In the propagation, it is instructive to note a few features which illustrate the importance of scattering off a potential that may not be intuitive due to the wavelike nature of quantum mechanics.

In Figure 7, the expectation value has reached the edge of the potential well. The shape of the Gaussian has changed as expected because some of the packet has reached this lower potential, and thus has gained energy. However, due to the wavelike nature of quantum mechanics, there has been some reflection off the potential change as well, resulting in interference in the packet even before the potential has been reached, and nonzero negative k.

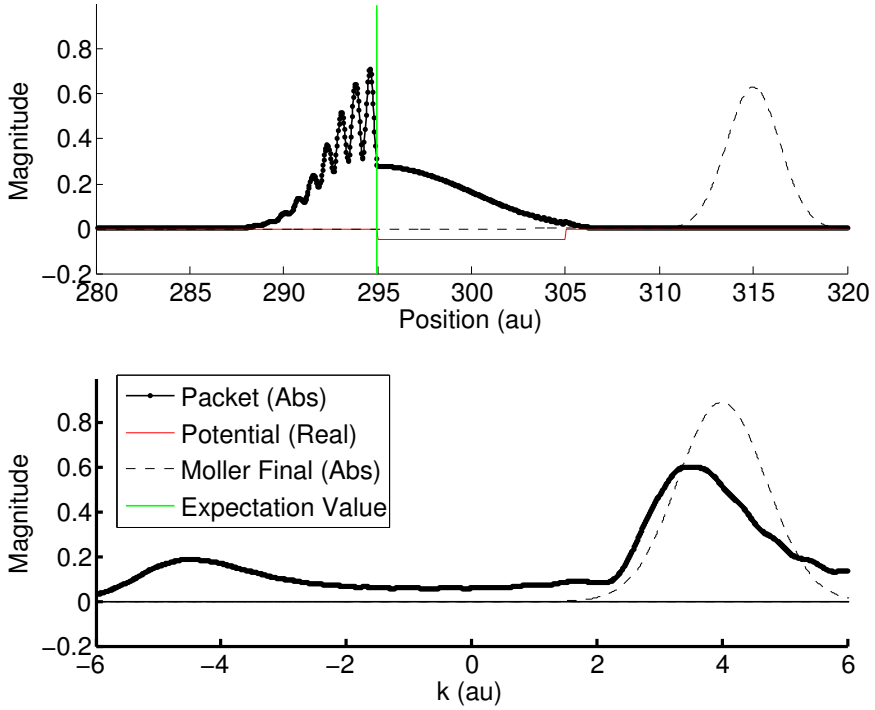

Figure 7. Propagation through square potential at time of 2200 au

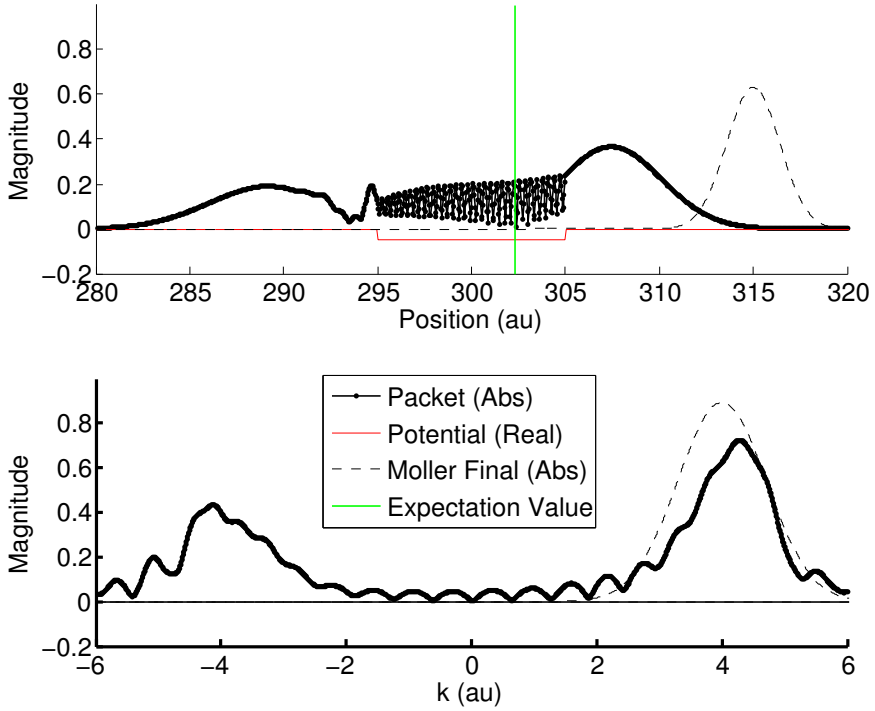

Figure 8. Propagation through square potential at time of 3700 au

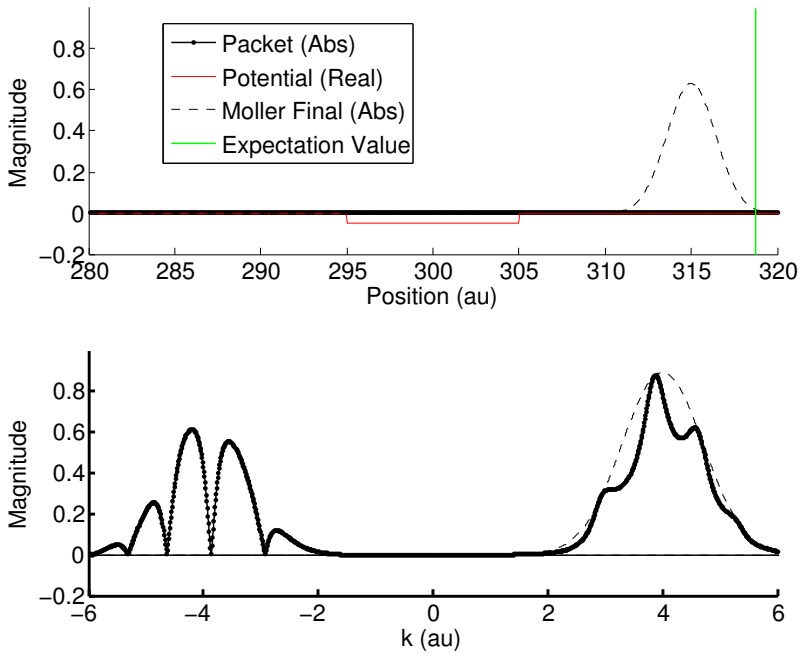

Figure 9. Propagation through square potential at time of 15000 au with transmission Møller state

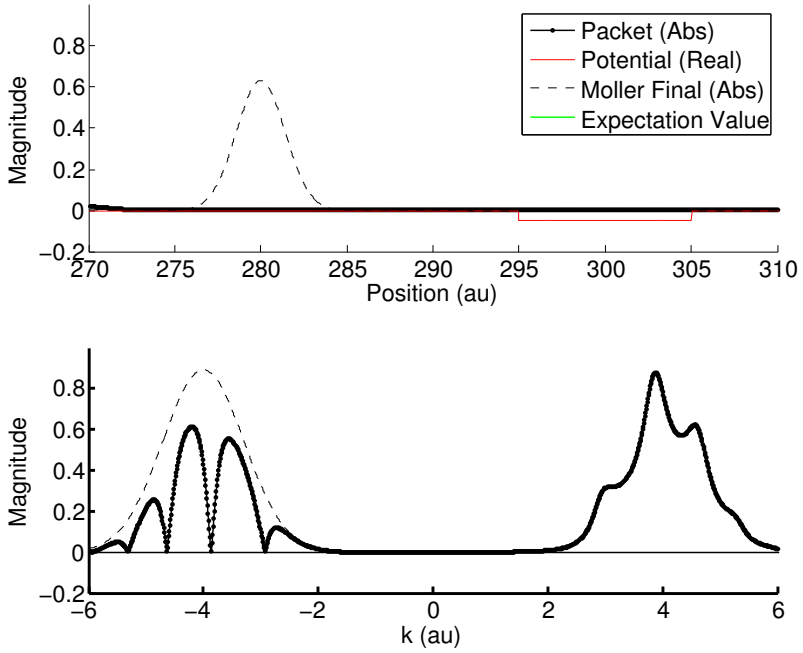

Figure 10. Propagation through square potential at time of 15000 au with reflection Møller state

In Figure 8, it is quite obvious that only some of the wave is being transmitted and some of the wave is being reflected. Interference is causing only certain k values to be present. Some of the packet is bouncing around inside the potential, while some of the packet has been able to escape from the potential. The resulting transmitted and reflected packets are taking shape, and the transmitted packet is beginning to reach the Møller final state.

Figures 9 and 10 show the propagation at final time with the transmission and reflection Møller final states, respectively. Under this set of parameters, the transmission Møller final state exactly matches the initial wave packet in k-space, and the reflection Møller final state is the same as the initial except at $-k$. The packet is, in each case, beyond the Møller final state in position space, and at no point does it possess more magnitude in $|k|$ than it originally had, illustrating the collision was elastic. Certain values of $|k|$ were reflected, while other values of $|k|$ were transmitted, depending on the structure of the square potential. Equations (33-34) may now be understood visually – it is the ratio of the current value with the initial value that provides the transmission coefficient (and similarly in $-k$ space, since it $E = \hbar^2 k^2/(2m)$, so the sign of k is irrelevent in determining the energy).

Figures 11 and 12 show the correlation function for transmission and reflection inputs, respectively. At each time step of the propagation, the result in position space is projected onto the Møller final state in position space, and this value is recorded as the value of $\langle \psi_- | e^{-i\hat{H}t} | \psi_+ \rangle$. As indicated by Equation (26), it is the Fourier transform of this function in energy space that provides the S-matrix elements.

Another interesting problem is encountered here from a numeric perspective. Equally spaced points in position and k are natural choices for the propagation of the wave packet. At each time step, two Fourier transforms are necessary in the Split Operator propagation scheme used, as shown in Equation (13). Therefore, it is

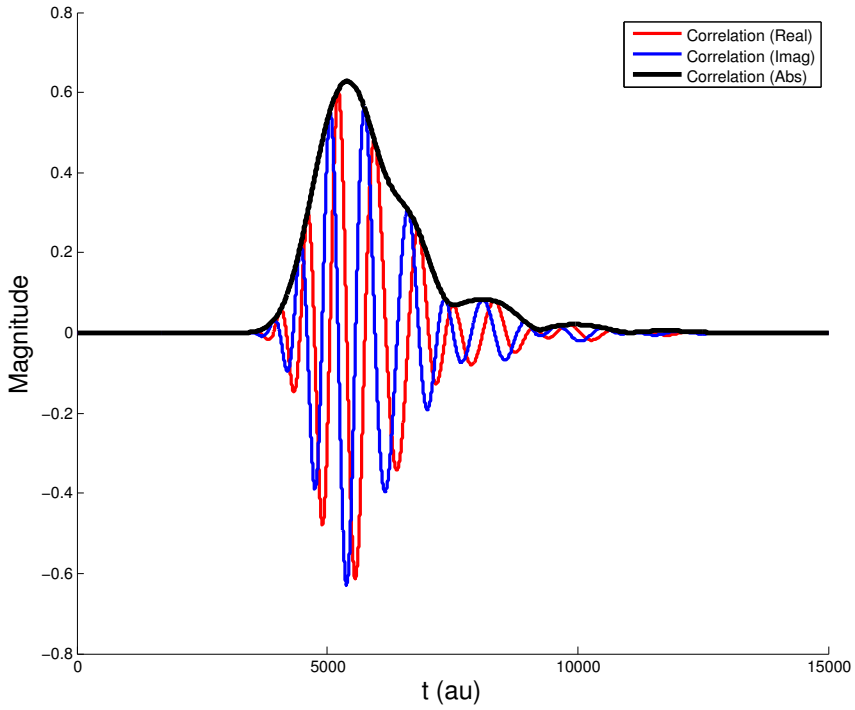

Figure 11. Correlation function of transmission through square potential

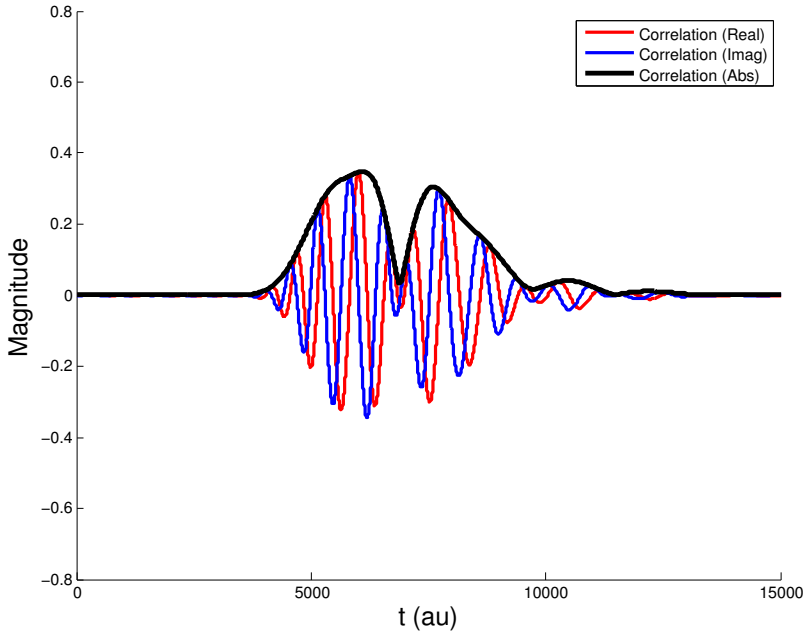

Figure 12. Correlation function of reflection off square potential

ideal to perform these Fourier transforms as rapidly as possible. The fastest known algorithm today is the Fast Fourier Transform, which relies on equally-spaced inputs.

However, when taking the inverse Fourier transform to calculate the S-matrix elements, this Fourier transform is in energy space. Since $E = \hbar^2 k^2/(2m)$, using equally spaced points in k means the Fast Fourier Transform cannot be applied in this calculation through standard techniques. There are three possible solutions to this problem:

- Equation (25) relies only on the expansion coefficients of the initial and final states, which we have assumed are Gaussian. The Fast Fourier Transform may be applied, and the necessary expansion coefficients may be calculated for each energy value using Equation (18). Although not generally applicable, the code already makes the assumption that the Møller states are Gaussian wave packets, and therefore are placed in the asymptotic limit of the potential.

- Since the Fourier transform of the correlation function is one-time work and the Fourier transforms for propagation are every iteration work, it is possible to maintain generality by simply using the full Fourier transform integral expression instead of the Fast Fourier Transform to compute the S-matrix elements, and use the Fast Fourier Transform for the much more frequent propagation calculations. This maintans generality, at the expense of some computational cycles. However, it was determined that the computational cost was not that great, so this approach was taken in the code in Appendix B.

- It seems plausible to modify the Fast Fourier Transform algorithm to work with data points spaced as $\sqrt{E}$, allowing both generality and speed to be preserved, but the details of this approach were not explored, as the runtime with the full Fourier transform for calculating scattering was negligible compared to the

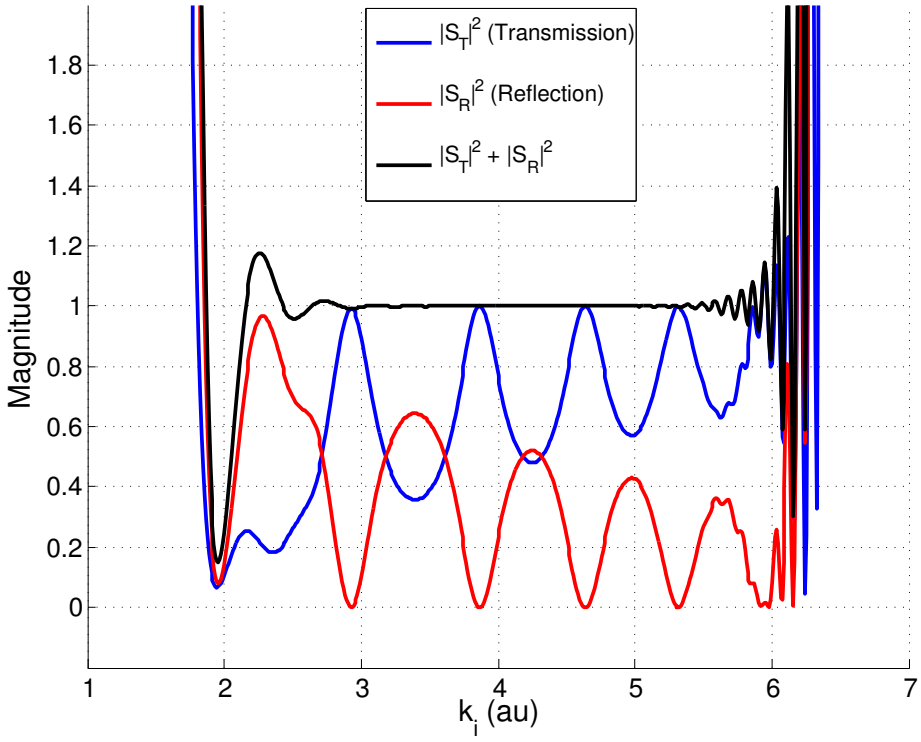

Figure 13. Square of the magnitude of S matrix elements from a square potential for transmission and reflection, and the sum, with $k_0 = 4$ and $\Delta k = 0.5$.

runtime for propagation.

Figure 13 shows the magnitudes of transmission and reflection along with the sum. Again, the data sums to 1 as expected near the central k value of $k_0 = 4$. Here, $\Delta x = 1$, so $\Delta k = 1/2$. The data is observed to be accurate from $k = 2.7$ to $k = 5.3$. Outside that range, the data deviates noticeably from this sum.

It is also possible to compare for a square potential using Equations (33) and (34). These results are plotted in Figures 14 and 15 for transmission and reflection calculations, respectively. Similar results are observed. Outside the range from $k = 2.7$ to 5.5 significant deviations begin to appear, at first gradually, then rapidly growing to overtake any semblance of a reasonable estimate of the actual value.s

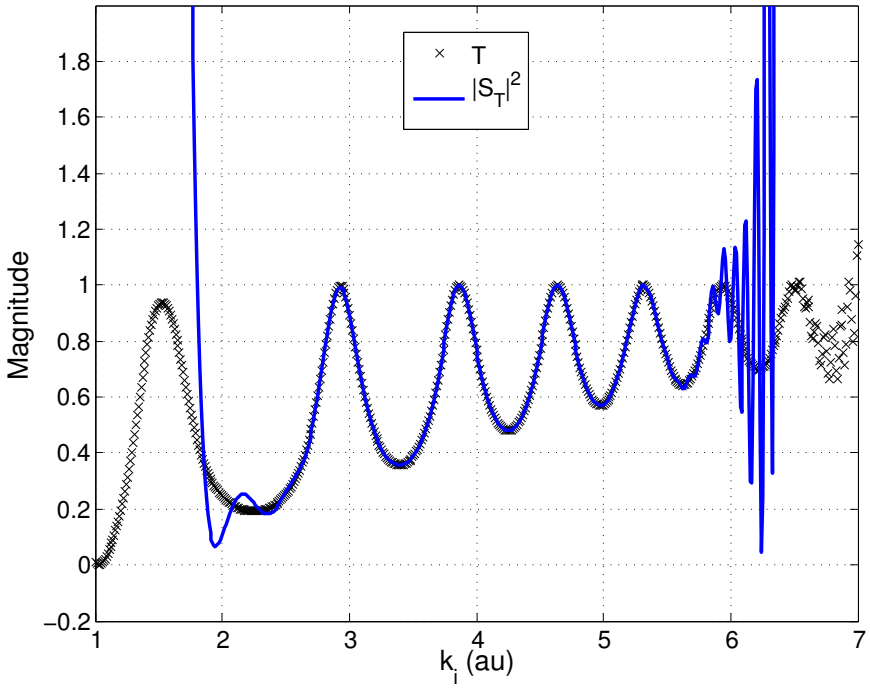

Figure 14. $|S_T|^2$ **compared to** T **from Equation (33) for a square potential, with** $k_0 = 4$ **and** $\Delta k = 0.5$**.**

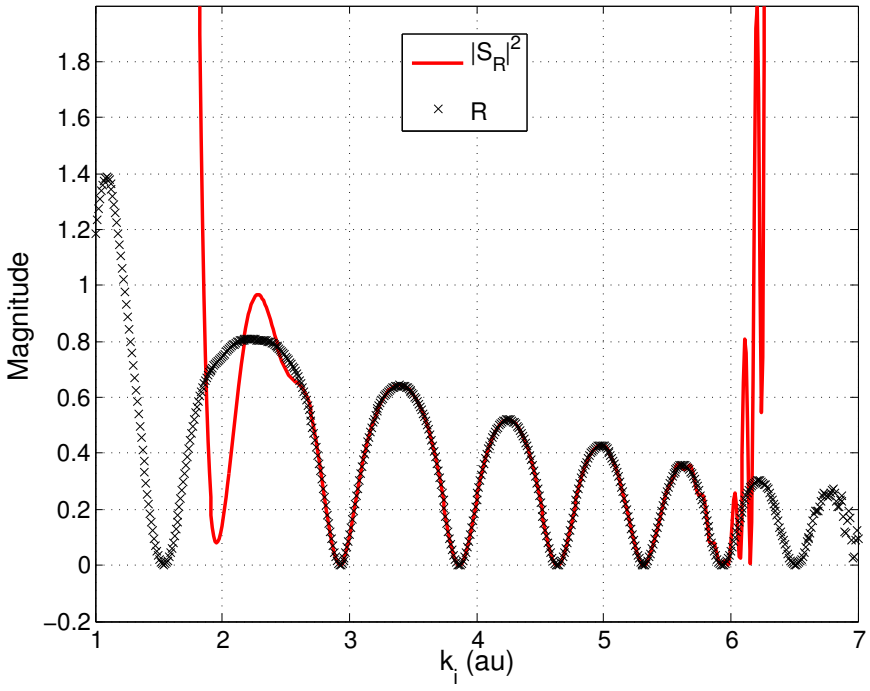

Figure 15. $|S_R|^2$ **compared to** R **from Equation (34) for a square potential, with** $k_0 = 4$ **and** $\Delta k = 0.5$**.**

4.4.3 Scattering Through a Spherical Central Potential.

For a spherical central potential, the procedure is similar, and a detailed example with coupling will be explored in Chapter V. The key difference is that scattering is completely reflective in this case. If there is no coupling, all scattering matrix elements should have a magnitude of 1, but the scattering angles will differ. Therefore, the calculation of scattering angles becomes essential for understanding scattering off a spherically symmetric central potential.

If coupling between multiple states is introduced, the magnitude of the scattering matrix elements may be less than 1, representing the transition from the starting state to another state. The magnitude of the S-matrix element quantifies the extent of the transition.

4.5 Cross Section Calculations

Cross section calculations follow naturally from the theoretical considerations previously discussed in Chapter III, with two minor modifications. First, the sums in Equations (29-31) are infinite, and the wave packet propagation for realistic potentials is generally the most computationally intensive step, so minimizing the required number of iterations in this sum while still converging to a reasonable answer is desired. Cohen-Tannoudji provided a method of truncating the sum [7].

From Equation (28), with increasing l, the point is reached where the following approximation holds:

$$V_{eff} \approx \frac{l(l+1)\hbar^2}{2mr^2} \tag{35}$$

When this point is reached, the potential $V(r)$ is no longer interrogated by a wave with energy k. Let r_{max} be the maximum r-value with non-negligible potential and

k_{max} is the maximum k-value (in absolute value):

$$\sqrt{l_{max}(l_{max}+1)} \approx k_{max} r_{max} \tag{36}$$

It is possible, depending on the exact potentials and wave packet dynamics, that the sum may be truncated sooner, when the contributions to the cross-section are below a certain threshold value. However, the above analysis provides a good starting point to estimate the cutoff for the sum for an arbitrary potential. By comparing the results for $l \approx l_{max}$, it is possible to determine whether the solution has converged or whether further propagations are required.

The other numerical issue in calculationg cross-sections is due to Equations (29-31). These equations are theoretically never negative, as expected, since a negative contribution to the cross-section makes no physical sense, but numerically, even for values near k_0, the magnitude of the S-matrix element may be slightly greater than 1, resulting in a computationally calculated negative cross section contribution. In order to avoid this effect, it is necessary to force the maximum value of the magnitude of the S-matrix elements to be 1. In Equations (29) and (30), it is not necessary to force the minimum value of the magnitude of the S-matrix elements to be 0, as $|S(k)|^2$ cannot be negative, even under ill numeric conditions.

4.6 Error Analysis

When considering error, it is of vital importance to recognize that error is a strong function of k (and therefore of $\sqrt{E}$) due to the presence of numerical error in the discretization process and chosen initial wave packet. The code contains many redundancies to help with error analysis as a function of k when outputting the results for the S-matrix and cross section calculations.

Some suggested ways to estimate algorithmic error are as follows:

- Calculate the S-matrix elements for all cases (reflection and transmission, elastic and inelastic) that are expected from the specified potential. The sum of the square of the magnitude for all S-matrix elements for a given k_i should be 1; deviations give a reasonable error estimate for $|S(k)|^2$ as a function of k.

- From the S-matrix elements, the total, absorption, and elastic cross sections are all calculated. Theoretically, this is redundant, as $\sigma_{tot} = \sum \sigma_{i \to j}$. This extra level of redundancy in output can also be checked to further estimate the error in the cross-section calculations. It is important to note that l_{max} may differ for σ_{el} and $\sigma_{i \to f}$. This method may only be used if both $\sigma_{i \to f}$ and σ_{el} have converged.

- In the code, the command-line option `-n=#` may be used to specify a minimal error tolerance; the default is $1e-10$. This specifies a lower bound on the error, although the actual error present is likely to be much larger than this value and depends on multiple parameters. Additionally, `-M=#` may be used to specify a user-defined value for l_{max}.

- Algorithmic error in propagation scales as $O(t^3)$. It is possible to estimate the magnitude of this propagation error by comparing the error in S-matrix elements calculated with $\Delta t = t_0$, then repeating the calculation with $\Delta t = t_0/2$.

- Propagator error may also arise from the spacing in position space and k-space. To reduce the spacing in k-space, it is necessary to sample over a larger space in x. To reduce the spacing in x-space, it is necessary to increase the number of data points.

V. Alkali-Noble Gas Scattering Cross Sections

5.1 Overview

In Diode Pumped Alkali Lasers (DPALs), collisional de-excitation between the $^2P_{3/2}$ and $^2P_{1/2}$ states is responsible for moving atoms from the upper pump state to the upper lasing state. To establish a population inversion necessary for lasing, this collisional transition should be maximized.

A reasonable approximation of the DPAL system is an alkali colliding with an inert gas. Although Rb and Cs are the most common alkalis for DPAL systems due to their large fine structure splitting, which allows pumping into the $^2P_{3/2}$ state without pumping the $^2P_{1/2}$ state, it is significantly more difficult to develop potentials for Rb-Noble Gas and Cs-Noble Gas systems. Therefore, in this section, LiHe will be considered.

Under this physical model, it was assumed that He is in its ground $^1S_0$ state, and Li was already in the excited $^2P_{3/2}$ state. Therefore, $E = 0$ will be set to the asymptotic energy of the $^2P_{3/2}$ state for convenience. Only fine structure coupling between the $^2P_{3/2}$ and $^2P_{1/2}$ states were permitted. Coupling between other states was neglected, and the hyperfine splitting of each fine structure state was ignored. This led to a two-state system.

The following tasks were performed:

- Calculate the cross sections for absorption, elastic collisions, and total collisions for LiHe by calculating S-matrix elements starting on the $^2P_{3/2}$ state and propagating through the LiHe potential.

- Calculate S-matrix elements for the inelastic $^2P_{3/2}$ to $^2P_{1/2}$ collision for a single effective potential with all other inputs the same. Sum with the S-matrix for elastic scattering to obtain a reasonable error estimate as a function of k.

5.2 Parameters

Estimated reasonable operating temperatures for the system are around $500\,K$. In particular, it would be desirable to obtain cross sections in the range from 300 to $1000\,K$, corresponding to energies of 0.000950050 to 0.00316683 Hartree. These results may then be convoluted with a distribution function to obtain experimentally significant results.

The atomic nuclear mass of Li is 12863.2 au, and He is 7349.67 au. This leads to a reduced mass of 4677.23 au. Under this mass, using $|k| = \sqrt{2mE}/\hbar$, $|k_{min}| = 2.98114$ and $|k_{max}| = 5.44280$. This indicates a wave packet centered at $k \approx -4.2$ with a width of $\Delta k \approx 0.65$, and therefore $\Delta x = 0.77 \approx 0.8$, is reasonable. The desired S-matrix elements are $S_{+k,-k}$ – the wave packet starts at large r where the potential is negligible, the propagates inward to small r ($-k$ direction) until it is reflected out (in the $+k$ direction). It must be remembered that the initial Gaussian must be negligible in $+k$ space for the Channel Packet Method to succeed, as shown in Table 2. Therefore, Δk cannot be made too large or a superposition of S-matrix elements will be obtained, as shown in Equation (27). Too small of a Δk is also bad, as shown in Chapter IV, as numeric error overtakes any computational accuracy beyond a range of roughly $k_0 \pm 3\Delta k$. Finally, it is desirable to get as many S-matrix elements in the energy range of interest with a single run of the Channel Packet Method in order to minimize propagation time, which is another reason to make Δk reasonably large, provided the overlap at $k = 0$ is negligible.

For a spherically symmetric problem, it is possible to estimate the propagation time required based upon the position of the initial packets and the minimum k value to obtain data for. Since $p = \hbar k$, it is possible to estimate the minimum velocity as $v_{min} = \hbar k/m$. Assuming the minimum position value is at $x = 0$ and the Møller initial and wave packets are at x_p, then a rough estimate of the time required can be

obtained by assuming constant velocity:

$$t_{max} \approx \frac{2x_p m}{\hbar k} \tag{37}$$

In actuality, since the effective potential for large l will slow down the wave packet, a somewhat larger value of t_{max} is generally required, but this gives a rough estimate of the value to use.

5.3 Potentials

The potentials are the most questionable part of the set of inputs for these LiHe calculations, and therefore the most likely source of error. Numerous attempts have been made to calculate the potentials for the LiHe interaction [15][16]. However, it is critical to note that these calculations generally include only the *adiabatic* potentials, and not the diabatic potentials or the interaction potential. Therefore, only part of the input set required is given in most papers. It is necessary to include a method of estimating the diabatic potentials from the adiabatic potentials. Fortunately, there is a method given in [10] and [11]. This method was applied to LiHe in [9]. The diabatic potentials provided in these sources are just an estimate, and depends upon knowledge of the crossing point of the diabatic potentials. For reasonable propagation parameters it is expected that error in this interaction potential (and thus the diabatic potentials) is the primary source of error in the cross section calculations.

There are a total of 6 states comprising the ^2P level. These states are the $^2P_{1/2,\pm 1/2}$, $^2P_{3/2,\pm 1/2}$, and $^2P_{3/2,\pm 3/2}$. In the adiabatic representation, these potentials form the $A^2\Pi_{1/2}$, $B^2\Sigma^+$, and $A^2\Pi_{3/2}$ states, respectively [9]. Therefore, to properly model this system, it appears a 6x6 matrix is required. This may be simplified into two block diagonal 3x3 matrices by assuming spin does not flip as a result of the collision. It is only necessary to solve one of these 3x3 matrices.

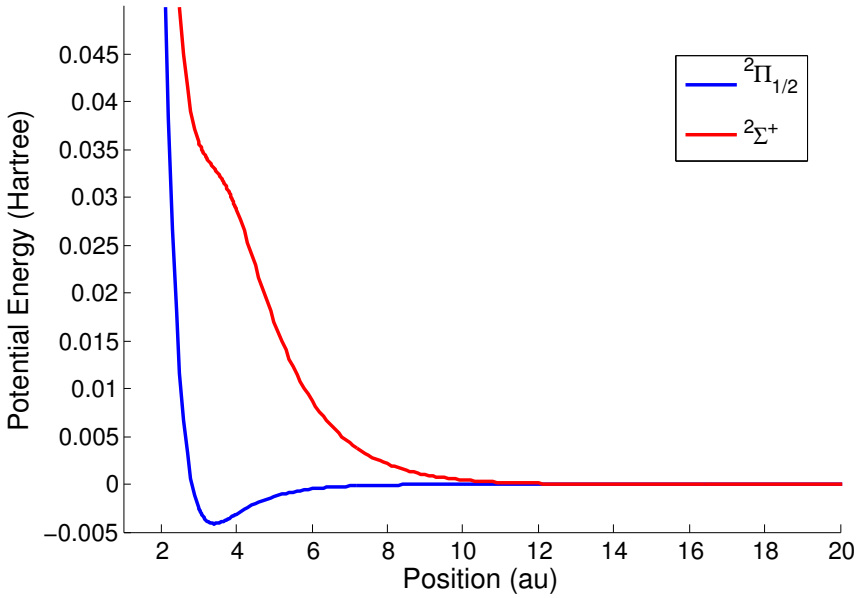

Figure 16. Adiabatic potentials for Li-He

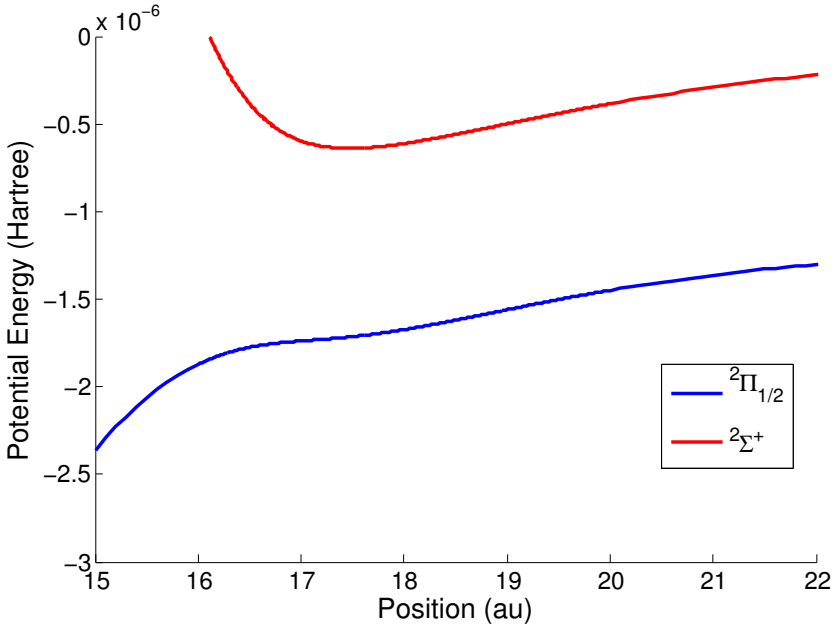

Figure 17. Adiabatic potentials used in propagation scheme, zoomed in at avoided crossing point

This may be further simplified by neglecting rotational (Coriolis) coupling [9]. This decouples the $A^2\Pi_{1/2}$ and $A^2\Pi_{3/2}$ states. It is sufficient to consider the following matrix of potentials (where each potential is a function of r):

$$\begin{bmatrix} V_{3/2,3/2} & V_{3/2,1/2} \\ V_{1/2,3/2} & V_{1/2,1/2} \end{bmatrix}$$

Here, the subscript 3/2 refers to the ${}^2P_{3/2,+1/2}$ state, and the subscript 1/2 refers to the ${}^2P_{1/2,+1/2}$ state. $V_{3/2,1/2} = V_{1/2,3/2}$, so a 2x2 symmetric matrix is obtained as described in Chapter II. The $V_{3/2,1/2}$ represents an approximation to the derivative coupling terms. The derivative coupling terms arise from the breakdown of the Born-Oppenheimer approximation. The eigenvalues of the 2x2 matrix are the adiabatic potentials. The eigenvectors of this matrix are described by a rotation matrix at each point in r:

$$C(r) = \begin{bmatrix} \cos(\theta(r)) & \sin(\theta(r)) \\ -\sin(\theta(r)) & \cos(\theta(r)) \end{bmatrix}$$

The adiabatic potentials chosen for use in this work were obtained from a Ph.D. student at the Air Force Institute of Technology and are pending publication [5]. The potentials are plotted in Figures 16 and 17. The avoided crossing occurs at 17 au, as illustrated clearly by Figure 17. From these potentials, it was possible to calculate an estimated interaction potential using the procedure in [9], [10], and [11]. It cannot be overemphasized that this procedure is approximate. In particular, Faist indicates the interaction potential is not very accurate for $r << R_x$, where R_x is the crossing point. Fortunately, this error should be relatively small, as the packet cannot propagate very far beyond the crossing point for low ($\approx 10^{-3}$ Hartree) energy.

The following equation for $\theta(r)$ was used[10][11]:

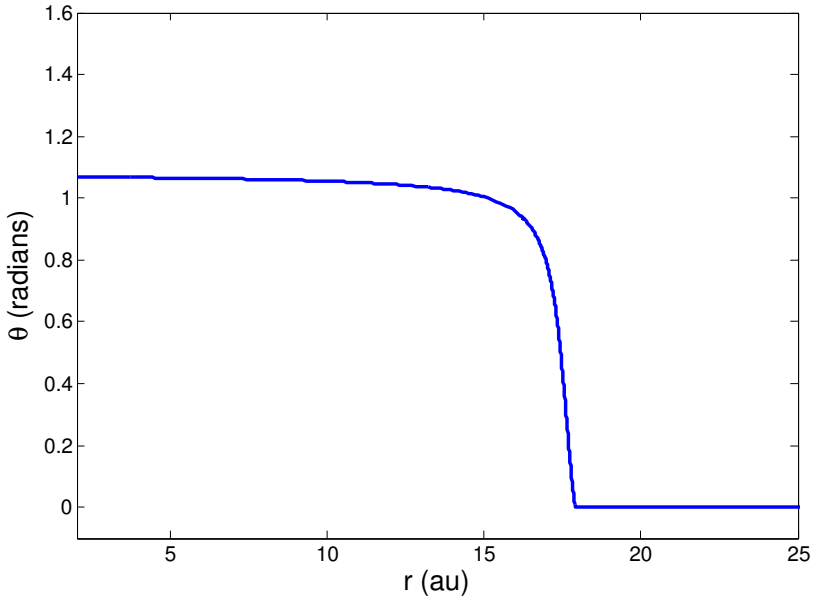

Figure 18. $\theta(r)$ **for estimating the diabatic potential from the adiabatic potential**

$$\theta(r) = \begin{cases} \frac{\pi}{4} + \frac{1}{2}\tan^{-1}(\gamma) - \frac{1}{2}\tan^{-1}(2\alpha(r - R_x) + \gamma) & \text{for } r \leq R_0 \\ 0 & \text{for } r > R_0 \end{cases} \tag{38}$$

where

$$R_0 = R_x + \frac{1}{2\alpha}\left[\tan\left(\frac{\pi}{2} + \tan^{-1}(\gamma)\right) - \gamma\right]$$

The parameters α and γ may be estimated from the difference potential. $\alpha = 1.2122$ and $\gamma = -1.484$ were used, with $R_x = 17$ for the crossing point. The potential near the crossing was well-behaved. However, the potential was strongly modified even far from the crossing point. $\theta(r)$ is plotted for the LiHe system in Figure 18.

5.4 Results

5.4.1 Propagation.

To begin exploring the cross section for the LiHe problem, the following propagation parameters were used:

```
-------------------------------------------------------------------------
Initial Gaussian Wave Packet Parameters
-------------------------------------------------------------------------
x0 = 4.0000000E+001    k0 =-4.2000000E+000    dx0 = 8.0000000E-001
m = 4.6772300E+003 (atomic units)
Packet all on Potential #1 initially
<x> = 4.0000000E+001
-------------------------------------------------------------------------
Moller Final State Parameters
-------------------------------------------------------------------------
x0 = 5.0000000E+001    k0 = 4.2000000E+000    dx0 = 8.0000000E-001
m = 4.6772300E+003 (atomic units)
Moller state on Potential #1
-------------------------------------------------------------------------
Hamiltonian Parameters
-------------------------------------------------------------------------
 Kinetic: Normal
# of potentials = 2

Potential #1

Potential: Interpolation (Linear Spline): ../LiHe_dia_p32_full_17.dat
Angular Momentum: l =  0
Boundary Conditions: Gaussian (Absorbing)
Mag = 1.0000000E+000    dx0 = 1.0000000E+001
Spherically Symmetric

Potential #2

Potential: Interpolation (Linear Spline): ../LiHe_dia_p12_full_17.dat
Angular Momentum: l =  0
Boundary Conditions: Gaussian (Absorbing)
Mag = 1.0000000E+000    dx0 = 1.0000000E+001
Spherically Symmetric
```

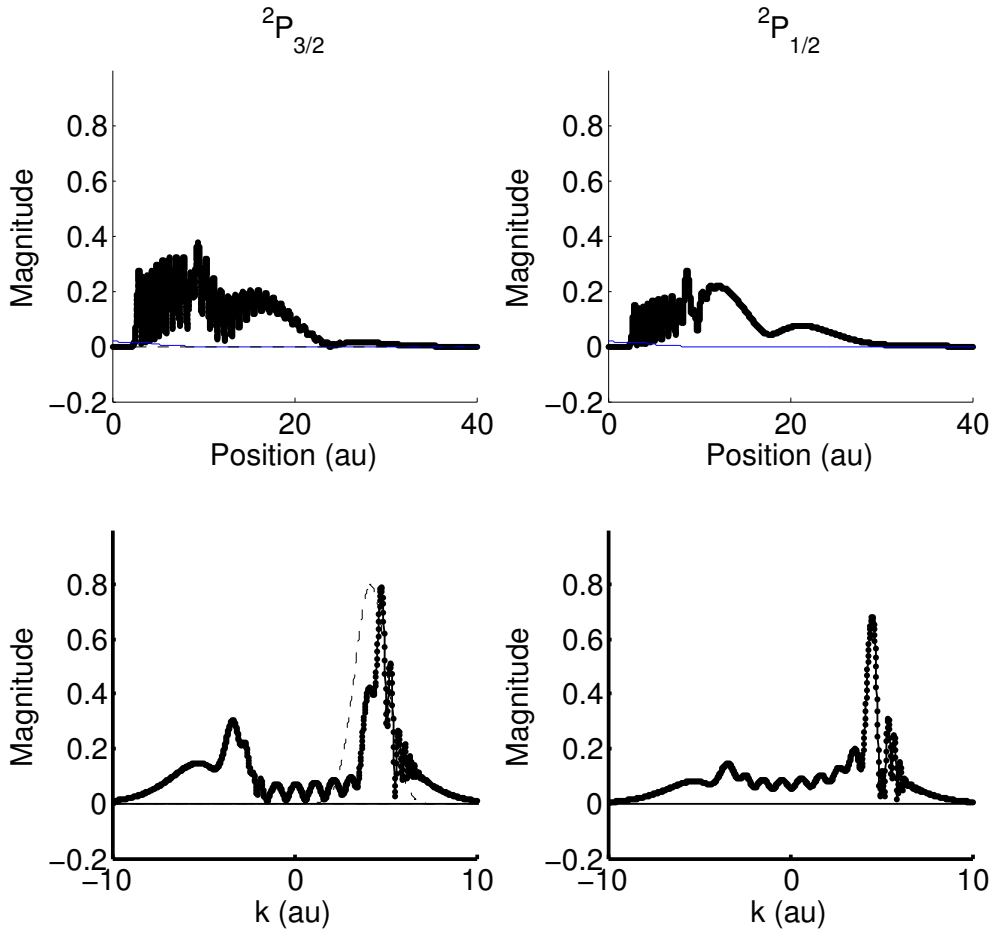

Figure 19. Propagation to $t = 45000$ au for $l = 0$. The absolute value of the initial momentum is the dashed line. The packet has mixed strongly due to the interaction potential.

```
Coupling Potential

Potential: Interpolation (Linear Spline): ../LiHe_dia_V12_full_17.dat
------------------------------------------------------------------------
Propagation Parameters
------------------------------------------------------------------------
x = 0.0000000E+000 to 3.2000000E+002; dx = 9.7659230E-003 (N = 32768)
k =-3.2166964E+002 to 3.2168927E+002; dk = 1.9634355E-002
t = 0.0000000E+000 to 4.0000000E+005; dt = 1.0000000E+000
(iterations: 400000)
------------------------------------------------------------------------
```

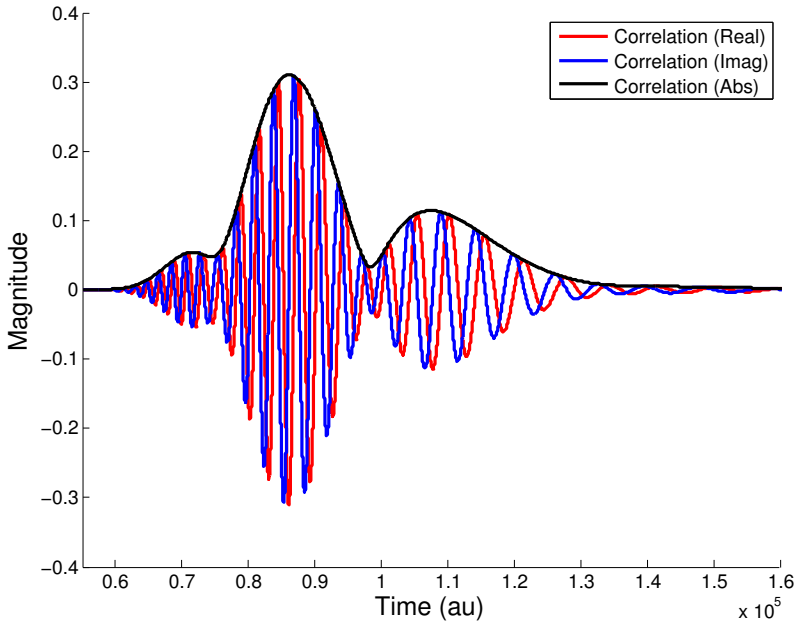

Figure 20. Correlation function for inelastic scattering with a Gaussian centered at 40 au.

Figure 19 contains intermediate results of the propagation for diabatic potentials calculated at $t = 45,000$ au for $l = 0$ (no effective potential). At this point in the propagation, a significant amount of mixing has occurred between the upper and lower states. Figure 20 shows the correlation functions from $t = 55,000$ to $160,000$ au, where the maximum correlation occurs on the inelastic state in all three cases. This reinforces the significant difference between the amount of wave packet transferred using each of the three methods of calculating the diabatic potential.

5.4.2 Scattering.

From the propagation parameters, scattering matrix calculations were obtained using the Channel Packet Method.

For the case of no effective potential modification ($l = 0$), the results are plotted in k-space in Figure 21, and in the more conventional energy space in Figure 22. It is advantageous to observe the behavior in both representations to perform error

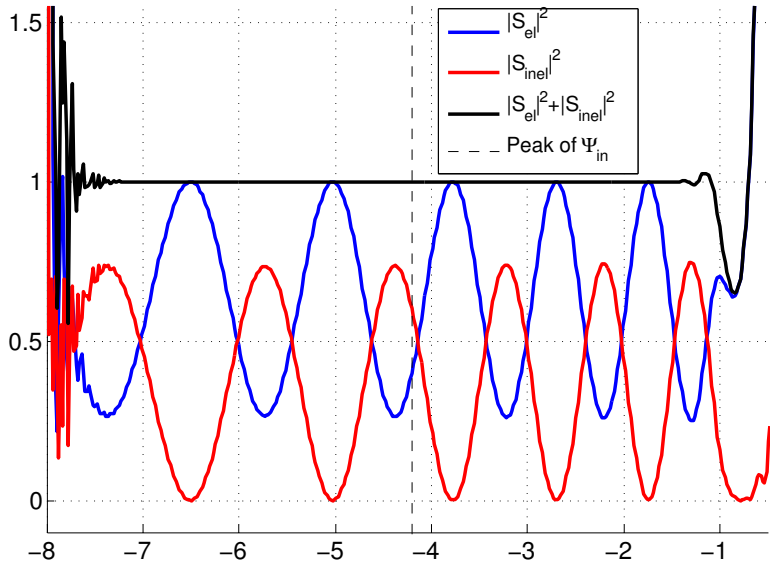

Figure 21. Magnitude of S-matrix elements as a function of k_i for $l = 0$ (no effective potential modification). The center value of the initial and final Møller states was $|k| = 4.2$.

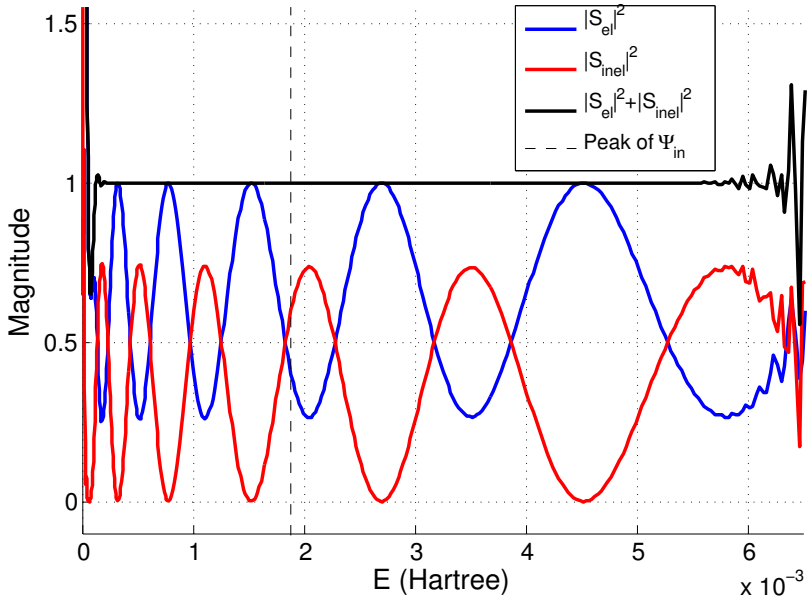

Figure 22. Magnitude of S-matrix elements as a function of E for $l = 0$ (no effective potential modification). The center value of the initial and final Møller states was $|k| = 4.2$ au, corresponding to $E = 0.001885$ Hartree.

analysis. In k-space, the points are equally spaced, and it is clear that the numeric error becomes significant at approximately $k_0 \pm 3$ au. In energy space, keeping in mind $E = (\hbar k)^2/(2m)$, the points are no longer equally spaced, so errors at larger energies (and thus large $|k|$) are somewhat magnified due to the relative sparsity of data points as compared to with small energy (and thus small $|k|$).

By examining the sum of the inelastic and elastic cross sections when $l \neq 0$, it was discovered that even for small effective potentials, the Gaussian shape was not a good approximation for the shape of the Møller state centered at 40 au. In Figure 23, the S-matrix elements for inelastic and elastic scattering do not always sum to 1.

In order to discover the reason for the failure for $l \neq 0$, using a more coarse calculation ($N = 4096$ and $x_{max} = 100$), the center of the Gaussian wave packet was moved to 30, 35, 40, and 50 au, respectively, for $l = 5$ and $l = 10$ to observe the effects on the scattering matrix elements. Also, a truncated effective potential was investigated, under the following form:

$$V_{eff,tr}(x) = \begin{cases} V_{eff}(x) & \text{for } x \leq x_c \\ 0 & \text{for } x > 0 \end{cases} \tag{39}$$

Here, x_c is the cutoff point for the potential. Figure 24 contains the results for $l = 5$, and Figure 25 contains the results for $l = 10$. In both cases, it is observed that the sum of the inelastic and elastic scattering matrix elements are 1 over a wider range as the wave packet is moved out, and for the truncated effective potential the results are exactly as expected.

This means the Gaussian wave packet is not a good approximation for the Møller initial and final states, even though the effective potential is very small in this region ($7.34e-6$ for $l = 10$ at $x = 40$). There are three different ways to handle this problem. The simplest solution is to move the wave packet out further. While this

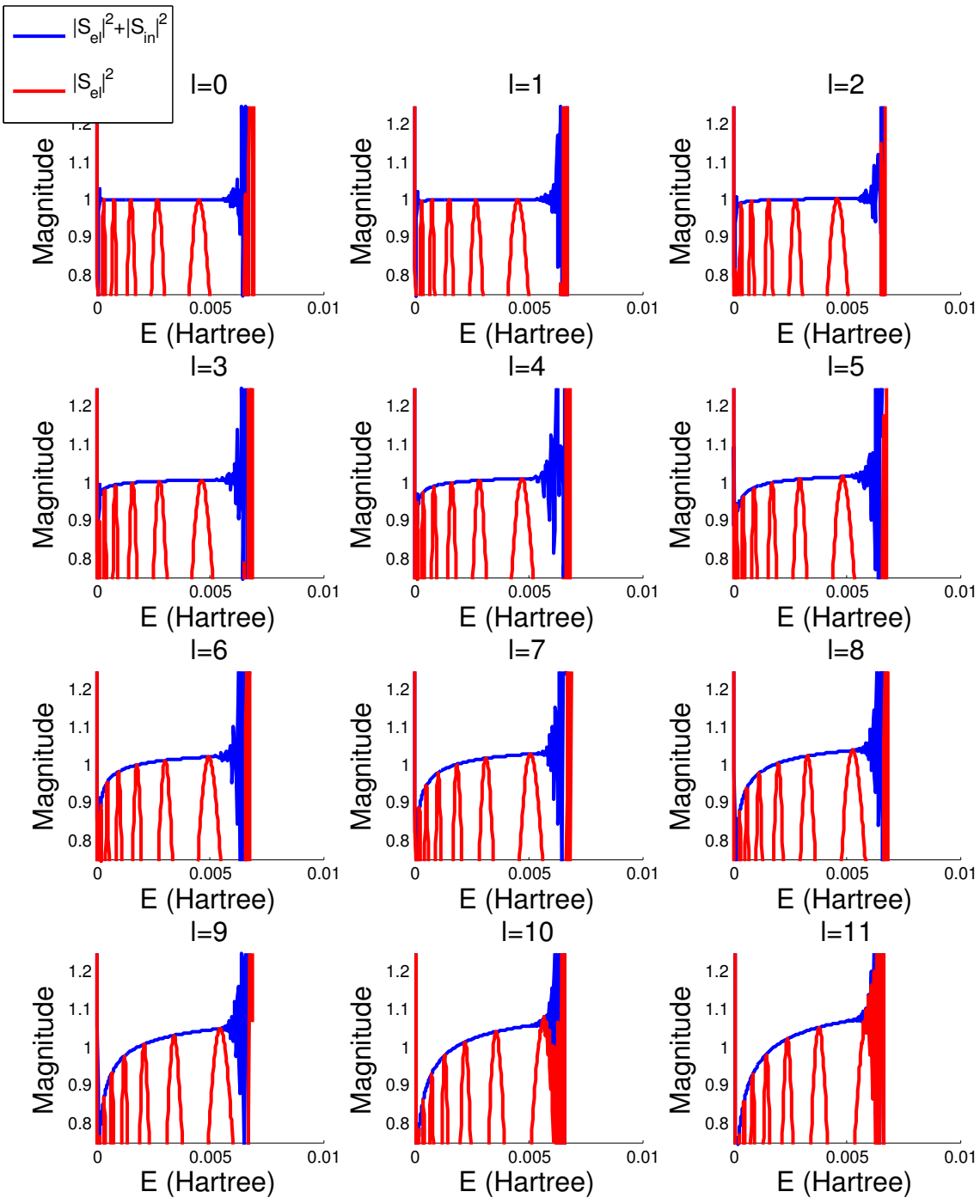

Figure 23. S-matrix elements with different effective potential l values, with a Gaussian centered at 40 au.

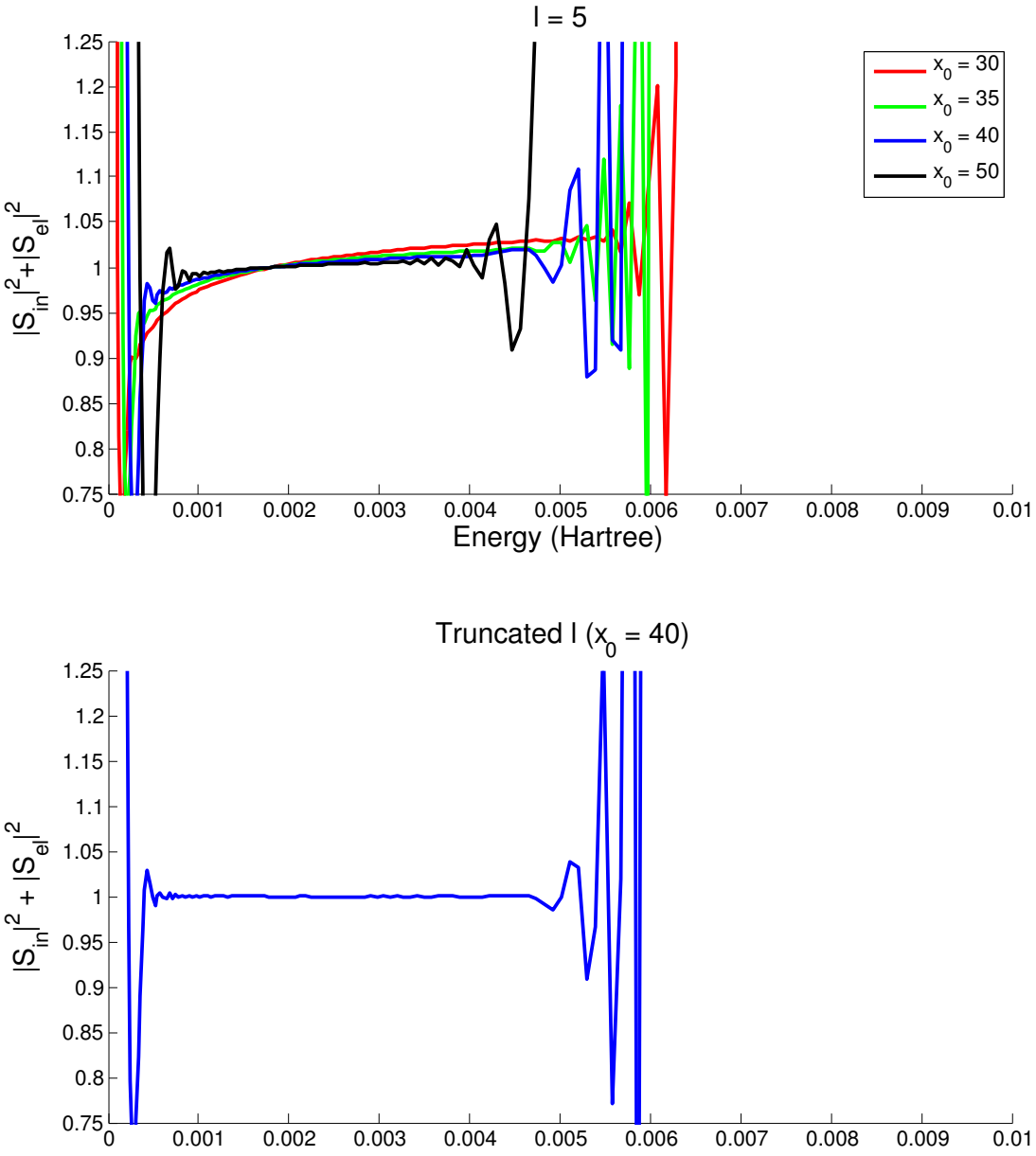

Figure 24. S-matrix elements for $l = 5$ with the Gaussian position varied.

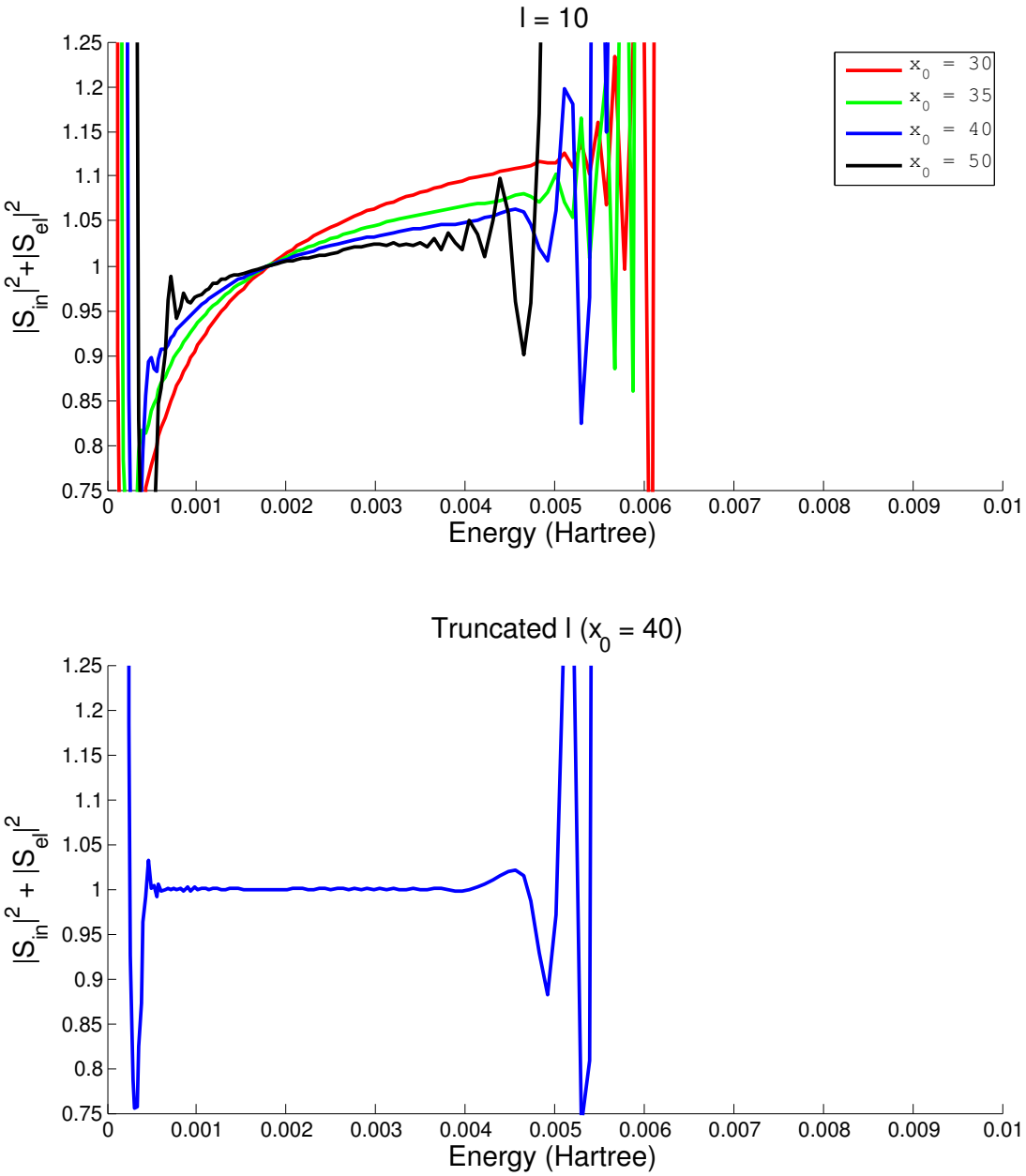

Figure 25. S-matrix elements for $l = 10$ with the Gaussian position varied.

solution appears simple on the surface, it was discovered that for the LiHe interaction, l values of around 100 were necessary to capture all of the absorption cross section data. Since the effective potential at a given point in space goes as $O(l^2)$, this would require moving the wave packet out substantially in space, resulting in a substantially longer propagation. Thus, this solution was not used.

Another possible solution is to develop the Møller state for each effective potential and use that potential for the initial Møller state. This must be done for all values of l that are required to perform the calculation. This reduces the propagation time problem, but requires more computational work up front to determine the initial Møller state.

Finally, a third solution is to simply truncate the effective potential as in Equation (39), which ensures the Gaussian is in fact a Møller state, at the expense of introducing some error from the modified effective potential. This error may be reduced by moving the wave packet farther out, where the effective potential is smaller. This solution was pursued by performing a second propagation.

5.4.2.1 Truncated Effective Potential.

For the truncated effective potential propagation, the following parameters were used:

```
------------------------------------------------------------------------
Initial Gaussian Wave Packet Parameters
------------------------------------------------------------------------
x0 = 5.0000000E+002    k0 =-4.2000000E+000    dx0 = 7.5000000E-001
m = 4.6772300E+003 (atomic units)
Packet all on Potential #1 initially
<x> = 5.0000000E+002
------------------------------------------------------------------------
Moller Final State Parameters
------------------------------------------------------------------------
x0 = 5.0000000E+002    k0 = 4.2000000E+000    dx0 = 7.5000000E-001
m = 4.6772300E+003 (atomic units)
```

```
Moller state on Potential #2
----------------------------------------------------------------------
Hamiltonian Parameters
----------------------------------------------------------------------
Kinetic: Normal
# of potentials = 2

Potential #1

Potential: Interpolation (Linear Spline): ../LiHe_dia_p32_full_17.dat
Angular Momentum: l =  0; r_max = 4.9000000E+002
Boundary Conditions: Gaussian (Absorbing)
Mag = 1.0000000E+000    dx0 = 7.0000000E+000
Spherically Symmetric

Potential #2

Potential: Interpolation (Linear Spline): ../LiHe_dia_p12_full_17.dat
Angular Momentum: l =  0; r_max = 4.9000000E+002
Boundary Conditions: Gaussian (Absorbing)
Mag = 1.0000000E+000    dx0 = 7.0000000E+000
Spherically Symmetric

Coupling Potential

Potential: Interpolation (Linear Spline): ../LiHe_dia_V12_full_17.dat
----------------------------------------------------------------------
Propagation Parameters
----------------------------------------------------------------------
x = 0.0000000E+000 to 6.0000000E+002; dx = 7.3251129E-002 (N = 8192)
k =-4.2877505E+001 to 4.2887976E+001; dk = 1.0470697E-002
t = 0.0000000E+000 to 5.0000000E+006; dt = 1.0000000E+001
(iterations: 500000)
----------------------------------------------------------------------
```

The key differences are: propagation over a longer time with a larger time step, fewer data points to accommodate the increased number of iterations, truncation for the effective potential above 490 au, and the wave packet and Møller final states centered at 500 au. The truncation ensured the initial and final Møller states were Gaussian. Since the packet was moved out significantly, the effect of truncation was

minimized. At 490 au with $l = 100$, the effective potential is $4.50e-6$ Hartree.

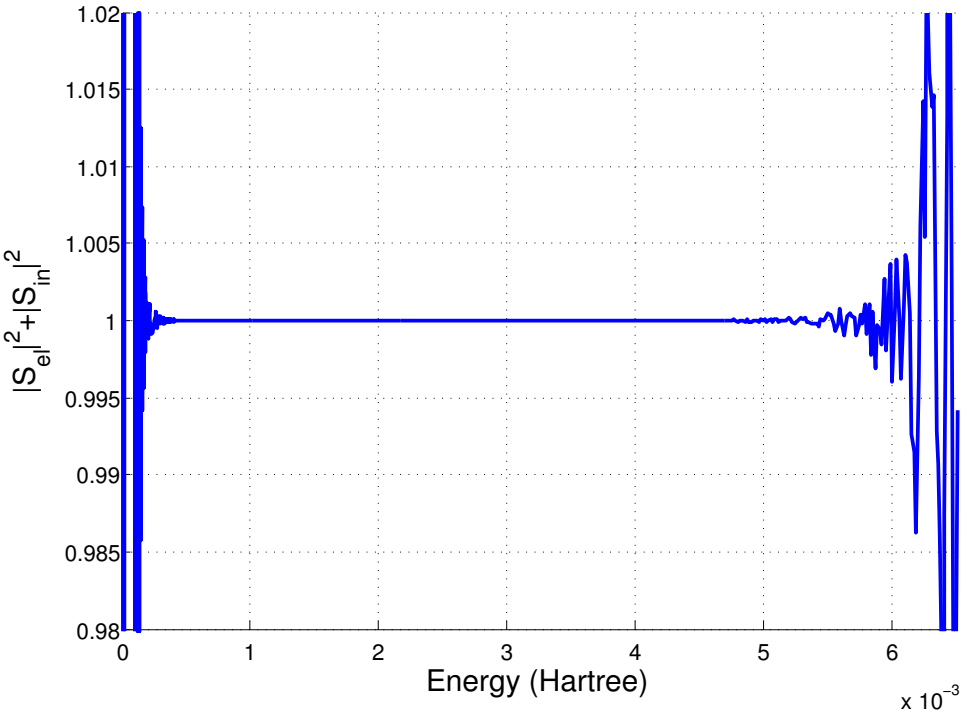

Figure 26. S-matrix element magnitude for $l = 0$, truncated effective potential above 490 au, and a Gaussian centered at 500 au.

To determine the numerically stable range for this new data set, the sum of the magnitude squared of the scattering matrix elements for $l = 0$ are plotted in Figure 26. From this figure, the region in which the data is valid to 3 significant figures is from 3e-4 to 5e-3 Hartree. This region will be referred to as the numerically stable region. Outside this region, the data is erroneous due to finite machine precision. Only within this region can the numeric error from using the Channel Packet Method be assumed to be less than 0.1%.

To confirm correct operation of the method, a comparison was made for the sum of the elastic and inelastic S-matrix elements at different l values. The effect of l on the results noted in the previous section was observed to completely vanish. Error was now entirely due to numeric considerations, as shown in Figure 27. Notice for

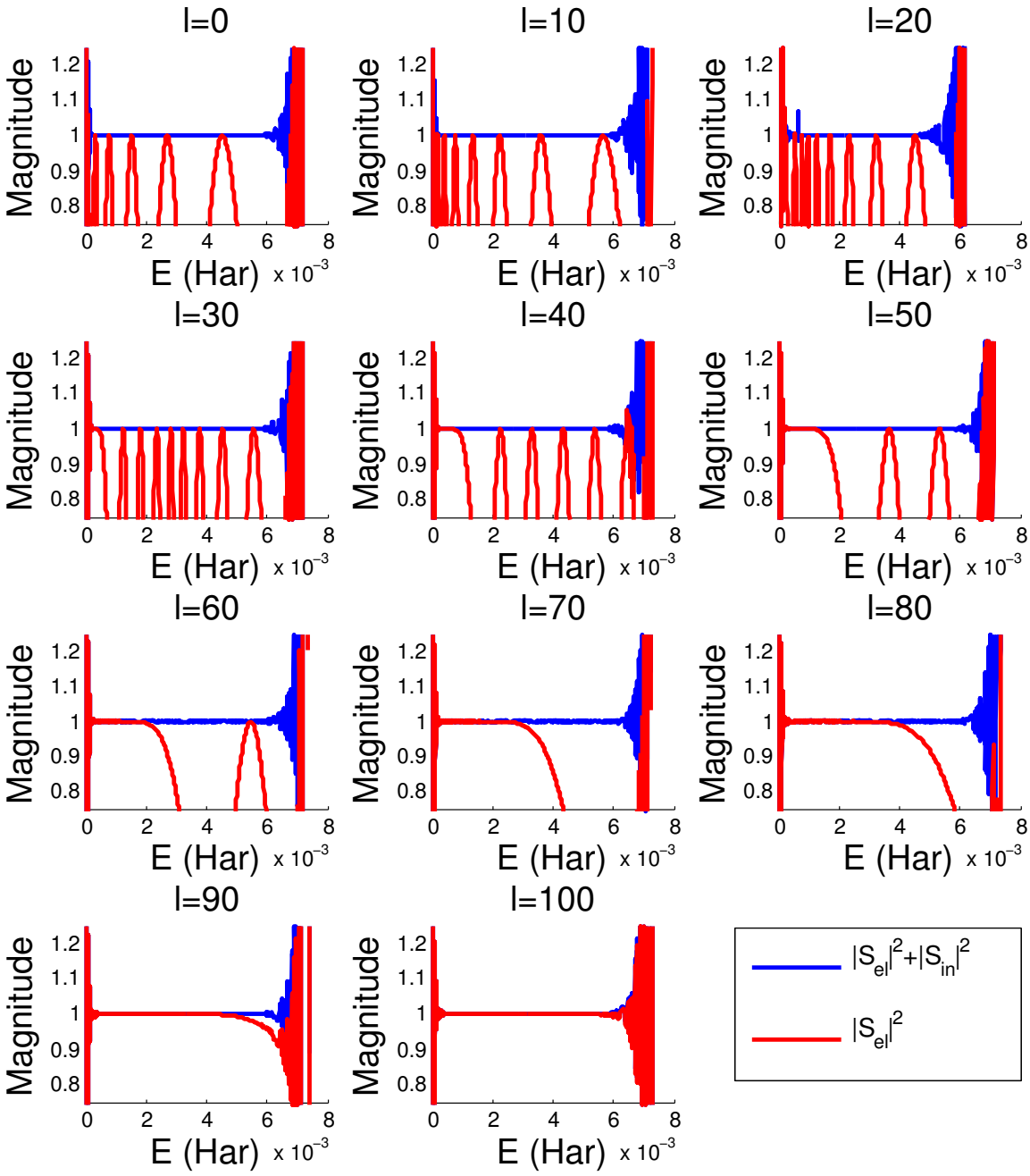

Figure 27. **S-matrix elements with different effective potential l values, truncated effective potential above 490 au, and a Gaussian centered at 500 au.**

$l = 100$, the elastic scattering magnitude is very close to 1 for all energies that are numerically stable, so this suggests $l = 100$ is a good cutoff point to truncate the summation given in Equation (30). For these potentials, the lower energies are the first to undergo purely elastic scattering, beginning at around $l = 40$, followed by the higher energies. Since S-matrix elements within the numerically stable region all summed to 1, the results of this propagation could be used to determine absorption cross sections.

5.4.3 Cross Sections (Derivative Coupling).

Elastic ($\sigma_{i\to i}$), inelastic ($\sigma_{i\to f}$), and total (σ_{tot}) cross sections were calculated using Equations (29), (30), and (31), respectively. To verify $l = 100$ is the proper cutoff point for the cross section calculations, the cross sections were calculated by setting l_{max} in increments of 10 – that is, $l_{max} = 0, 10, 20, ..., 100$. The results for the absorption cross section are presented in Figure 28. As expected, the low energies converge for smaller l_{max} than the high energies, since a smaller effective potential will cause the lower energies to be reflected.

By examining the elastic and total cross sections, it was clear that they had not yet converged to their actual value for any energies. Therefore, only absorption cross sections are reported. It is the absorption cross section which is of primary interest in the state transition, so this has minimal effect on the results. It was discovered that it is necessary to go to much higher l_{max} to obtain elastic and total cross sections for the LiHe potentials specified.

5.5 Analysis of Derivative Coupling Approximation

The general trend for the collisional absorption cross section is decreasing with increasing temperature. Since the absorption cross section is a convolution of this

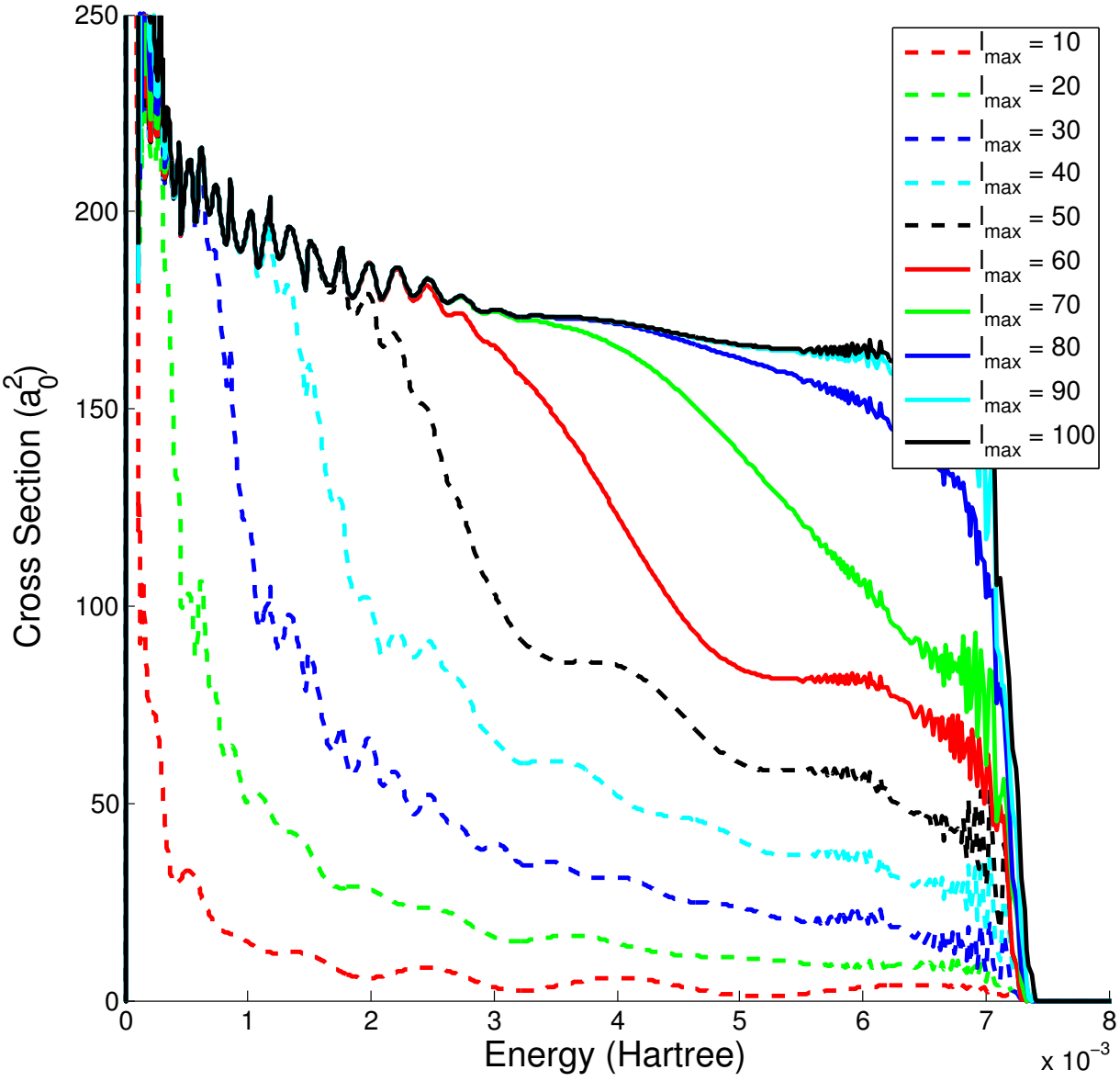

Figure 28. $\sigma_{i\to f}$ **calculated from cross section matrix elements for various cutoff points. For** $l_{max} = 100$**, the cross sections have converged.**

graph with the Boltzmann distribution and the resonant peaks are relatively narrow, it would be difficult to focus the energy only in one of the peak resonances. However, the collisional cross section should increase with decreasing temperature in general. This effect is not so great for temperatures above 1000 K, as the decrease in absorption cross section becomes much less dramatic beyond that temperature. However, the closer to room temperature the system is operated, the larger the collisional cross section becomes.

Although these qualitative observations agree reasonably with literature, at this point a more conventional means of obtaining the coupling between two states was discovered, and this method was disbanded at this point. The problem with the derivative coupling approximation method used was that the derivative coupling is hypothesized to be present only near the crossing point, but the approximation yielded derivative coupling terms far from the crossing point. Therefore, a more straightforward radial coupling method was used.

5.6 Radial Coupling Between States

There are 3 primary forms of coupling between the $^2P_{3/2}$ and $^2P_{1/2}$ states. These forms of coupling are: derivative coupling (examined by approximation in the previous section), Coriolis coupling, and radial coupling [9]. Coriolis coupling and derivative coupling are both neglected in this section. The formulation herein draws heavily from Alexander [2].

5.6.1 Theory.

Assume the potentials without spin-orbit splitting are calculated. In the P-level, this would yield 2 non-unique potentials which will be referred to as W_Π and W_Σ. The effect of adding spin-orbit splitting is offset each of these potentials by $3a/2$.

All of these variables are a function of r in the general case, although the spin-orbit splitting a may be approximated as a constant equal to the value in the asymptotic limit. Ignoring Coriolis coupling and derivative coupling, and examining only $\Omega > 0$ (since $\Omega < 0$ differs only by a negative sign in the off-diagonal $V_1 2$ elements), the potential is as follows:

$$\mathbb{V} = \begin{bmatrix} W_\Pi + \frac{a}{2} & 0 & 0 \\ 0 & \frac{1}{3}(2W_\Pi + W_\Sigma) + \frac{a}{2} & \frac{\sqrt{2}}{3}(W_\Pi - W_\Sigma) \\ 0 & \frac{\sqrt{2}}{3}(W_\Pi - W_\Sigma) & \frac{1}{3}(W_\Pi + 2W_\Sigma) - a \end{bmatrix} \tag{40}$$

It is important to note that coupling in this case reduces to simply a 2x2 matrix where only the electronic angular momentum $|J = 3/2, \Omega = 1/2\rangle$ and $|J = 1/2, \Omega = 1/2\rangle$ couple together, as follows:

$$\mathbb{V} = \begin{bmatrix} V_{11} & V_{12} \\ V_{12} & V_{22} \end{bmatrix} = \begin{bmatrix} \frac{1}{3}(2W_\Pi + W_\Sigma) + \frac{a}{2} & \frac{\sqrt{2}}{3}(W_\Pi - W_\Sigma) \\ \frac{\sqrt{2}}{3}(W_\Pi - W_\Sigma) & \frac{1}{3}(W_\Pi + 2W_\Sigma) - a \end{bmatrix} \tag{41}$$

Similar results (with the exact same eigenvalues) are observed for $\Omega = -1/2$. In the radial approximation, the $|3/2, \pm 3/2\rangle$ state does not couple at all with the $|1/2, \pm 1/2\rangle$ states. Coriolis coupling is responsible for coupling these two states, which is neglected in this thesis. Therefore, the cross section may be calculated using this 2x2 matrix.

In order to obtain a cross section for the ${}^2P_{3/2} \rightarrow {}^2P_{1/2}$ transition, it is necessary to combine the cross sections in some manner. This depends upon the population distribution among the hyperfine states. If the hyperfine distribution were confined to the $|3/2, \pm 3/2\rangle$ state and radial coupling were the only mechanism present, the cross section would obviously be 0. On the other hand, if the hyperfine distribution were confined to the $|3/2, 1/2\rangle$ state, the cross section for the transition would equal

the cross section for the $|3/2, 1/2\rangle$ state to transition to either of the $|3/2, \pm 1/2\rangle$ states. Thus, the question of finding the fine structure cross section depends upon the population distribution among the hyperfine states, since the coupling mechanisms between each hyperfine state (and therefore the cross sections for each hyperfine state) differ.

In the general scenario, if the hyperfine population distribution is assumed to be $P(3/2, \Omega)$, the following equation holds:

$$\sigma_{3/2\to 1/2}(E) = \sum_{\Omega=-3/2}^{3/2} P(3/2, \Omega)[\sigma_{3/2,\Omega\to 1/2,1/2}(E) + \sigma_{3/2,\Omega\to 1/2,-1/2}(E)] \tag{42}$$

In the radial coupling approximation, $\sigma_{3/2,1/2\to 3/2,1/2} = \sigma_{3/2,-1/2\to 3/2,-1/2}$ and all other cross sections are 0, since there are no coupling (off-diagonal) terms in the potential. Therefore, assuming equal hyperfine splitting ($P(3/2, \Omega) = 1/4$):

$$\sigma_{3/2\to 1/2}(E) = \frac{1}{2}\sigma_{3/2,1/2\to 1/2,1/2}(E) \tag{43}$$

It is therefore sufficient in the radial coupling approximation to find $\sigma_{3/2,1/2\to 1/2,1/2}(E)$, keeping in mind that the approximated cross section for the fine structure transition is simply half of that value if the population is distributed equally among the hyperfine states.

5.6.2 Cross Sections (Radial Coupling).

The hyperfine cross sections $\sigma_{3/2,1/2\to 1/2,1/2}(E)$ were calculated for Li + ^{4}He, Li + ^{3}He, Na + ^{4}He, K + ^{4}He, and ^{85}Rb + Ar using the method outlined in the previous section, except with the potential given by Equation (41).

The results for Li colliding with different isotopes of He are plotted in Figure 29.

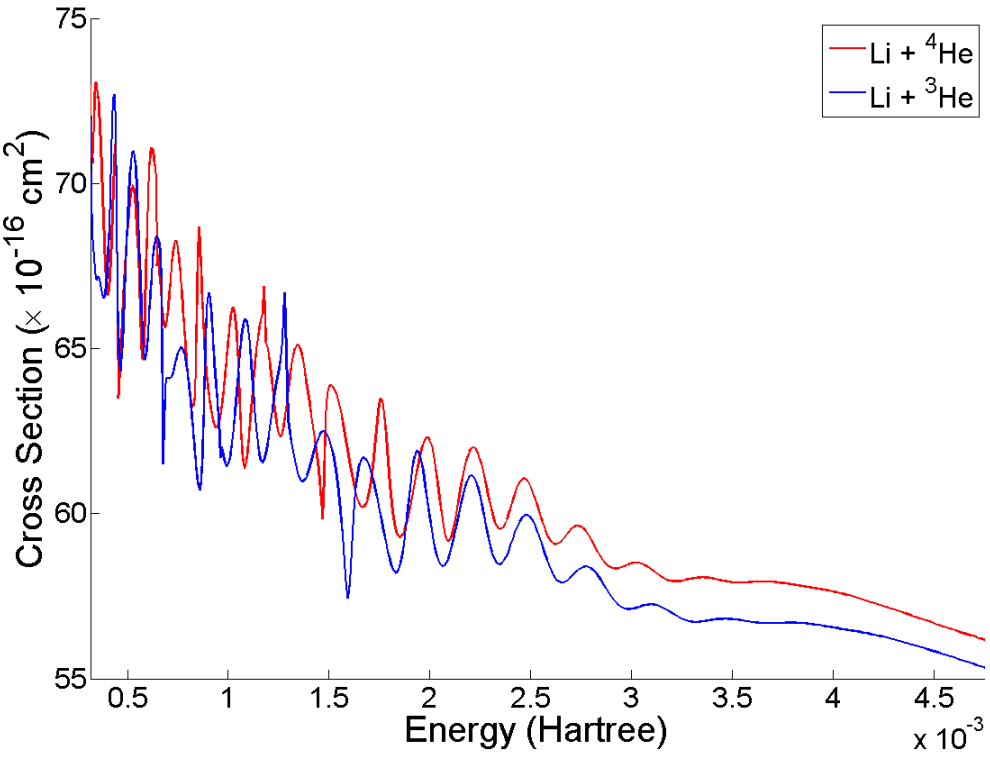

Figure 29. $\sigma_{3/2,1/2\to 1/2,1/2}$ **for Li +** ^{4}**He and Li +** ^{3}**He**

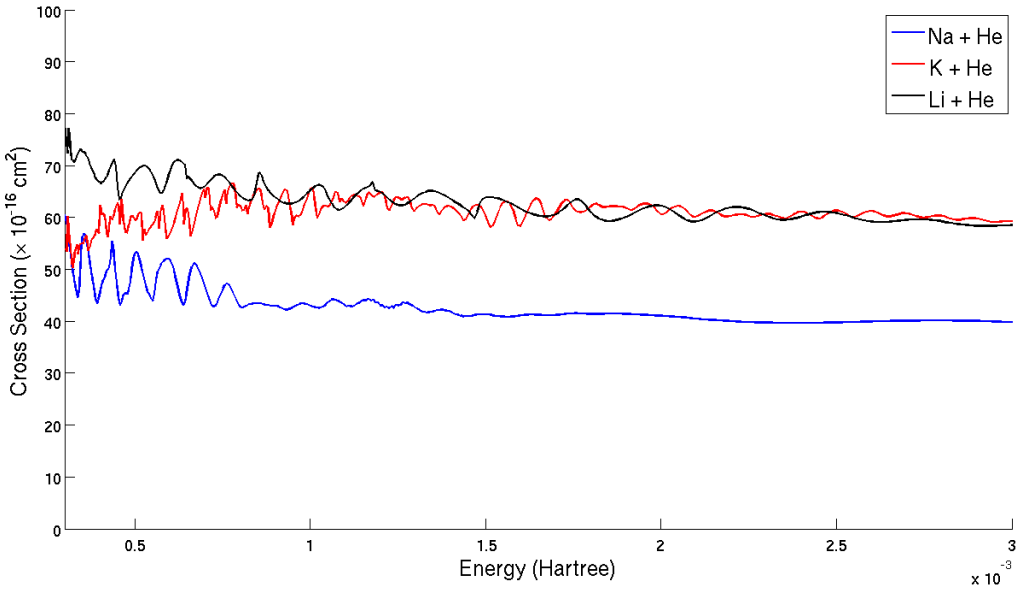

Figure 30. $\sigma_{3/2,1/2\to1/2,1/2}$ **for Li + ^{4}He, Na + ^{4}He, and K + ^{4}He**

There is not a significant variation with increased mass, although the cross section for Li + ^{4}He is approximately 1.5% higher than the cross section for Li + ^{3}He. The potentials do not vary from one calculation to another. This suggests that cross sections in the radial coupling approximation *may* be improved slightly by selecting the heavier of two isotopes when a choice is available. Further investigation is required to determine whether this result is specific to Li + He or whether this is a general phenomenon.

Results for Li + ^{4}He, Na + ^{4}He, and K + ^{4}He are plotted in Figure 30. In the radial coupling approximation, there is no significant variance in the results, particularly for Li + He and K + He.

The results for ^{85}Rb + Ar are plotted in Figure 31. Here, the cross section is significantly lower than the cross sections calculated for other isotopes, by approximately a factor of 10^{-5}.

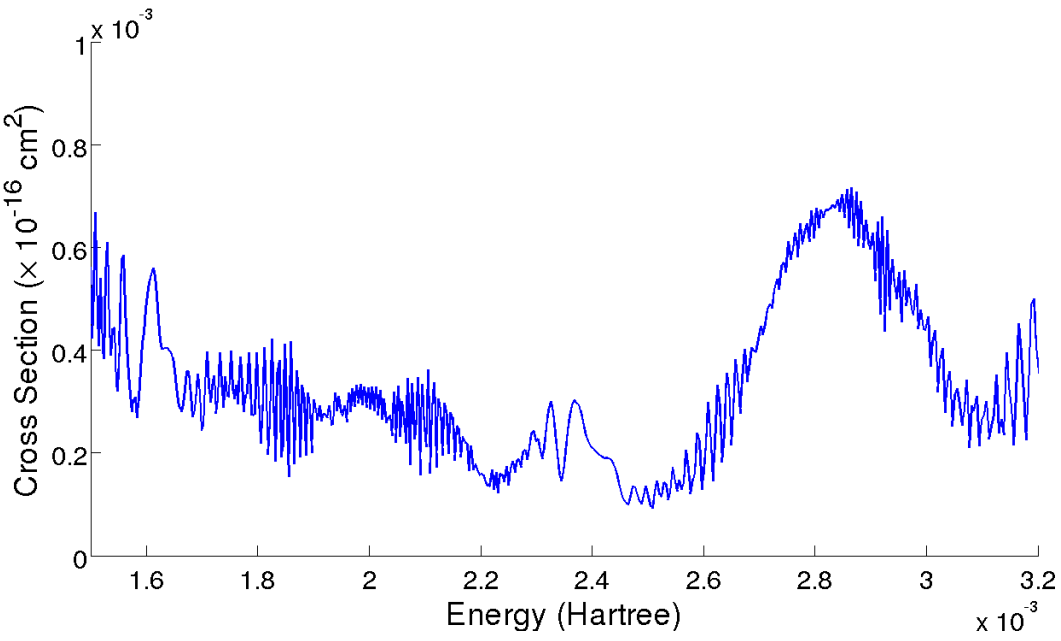

Figure 31. $\sigma_{3/2,1/2\to1/2,1/2}$ **for** ^{85}**Rb + Ar**

5.6.3 Comparison to Experimental Values.

There are some key differences between theoretical cross section calculations and experimental measurement of cross sections. The cross sections calculated from experiment would be the thermal average of the cross sections calculated in the previous section, and therefore would not be expected to exhibit rapid oscillations. Furthermore, assuming the hyperfine population of the $J = 3/2$ level are all equally populated, the experimentally observed cross section is half the result calculated for the hyperfine $\sigma_{3/2,1/2\to1/2,1/2}$ transition, as described in Equations (42) and (43).

It was difficult to obtain accurate experimental comparisons against values in the literature for the cross sections for LiHe. One of the difficulties is that the fine structure splitting of Li is so small, so it compounds the experimental difficulty of such a determination. It is possible to get a reasonable estimate, though. In [9], the cross section for the fine structure transition is listed as 37.3×10^{-16} cm^2 (or 37.3

Å^2) at 556 K. Cross sections for the $^2P_{3/2} \rightarrow {}^2P_{1/2}$ collision with other noble gases are given as falling in the range from 31.4 Å^2 (LiNa) to 66.0 Å^2 (LiXe) at this same temperature.

When the results for Li + ^{4}He in Figure 29 are convolved with a Boltzmann distribution at 556 K and divided by 2 as per Equation (43), the result computed is $31 \times 10^{-16}\, cm^2$, which is somewhat lower than the experimental value of $37.3 \times 10^{-16}\, cm^2$, but relatively close. The results are expected to be somewhat low, since derivative coupling and Coriolis coupling were completely ignored, though, so this is not a problem.

For Na + He, the calculated results are again relatively close to experiment, although slightly lower if the hyperfine distribution is assumed to be equal. Experimental cross sections are given at 385 K as $46.0 \times 10^{-16}\, cm^2$, and at 300 K as $37.7 \times 10^{-16}\, cm^2$ [16]. The results calculated in this thesis yield cross sections of $21.5 \times 10^{-16}\, cm^2$ at 385 K and $21.4 \times 10^{-16}\, cm^2$ at 400 K, respectively. Again, it is observed that the cross sections are in the right ballpark, but are a bit low, since derivative coupling and Coriolis coupling were both neglected.

Finally, experimental results for this collisional transition in Rb + Ar are difficult to calculate precisely since the transitions are relatively small, but are around $1 \times 10^{-3} \times 10^{-16}\, cm^2$ at 340-400 K, as summarized in [17]. This is again in the same order of magnitude as the results from these calculations, although again these calculations are observed to be somewhat less due to neglecting derivative and Coriolis coupling.

The calculation of time dependent results for Rb + Ar allow one to explore the reasons why it couples so much worse than the Alkali + He results. The diabatic potentials for Li + He are plotted in Figure 32, and the diabatic potentials for Rb + Ar are plotted in Figure 33. There are two factors which jump out as explanations of this result. First, the coupling (off diagonal) term in the potential is significantly

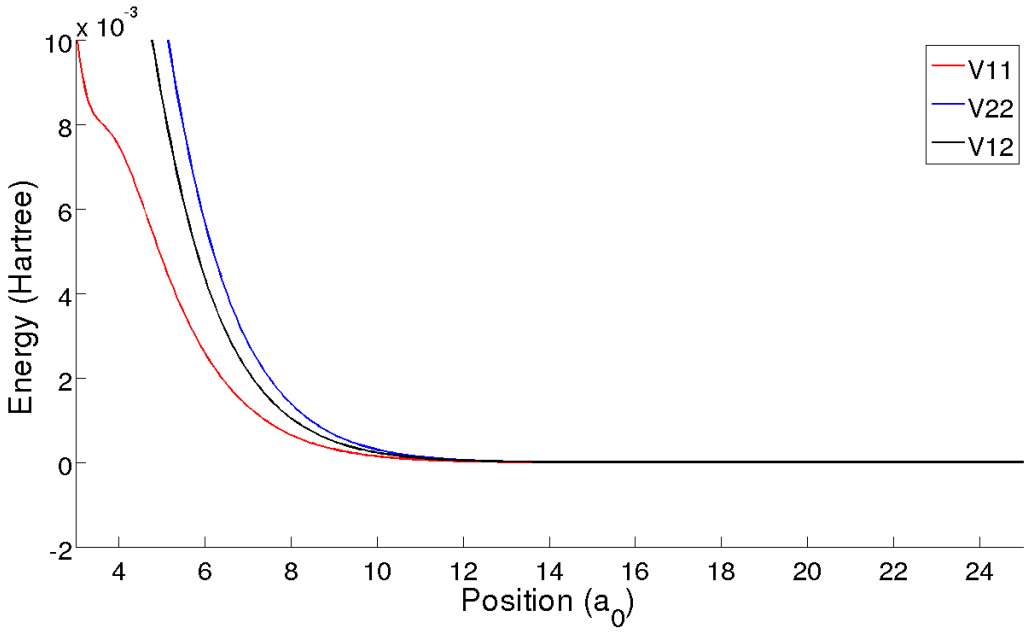

Figure 32. Potentials for Li + He (diabatic representation).

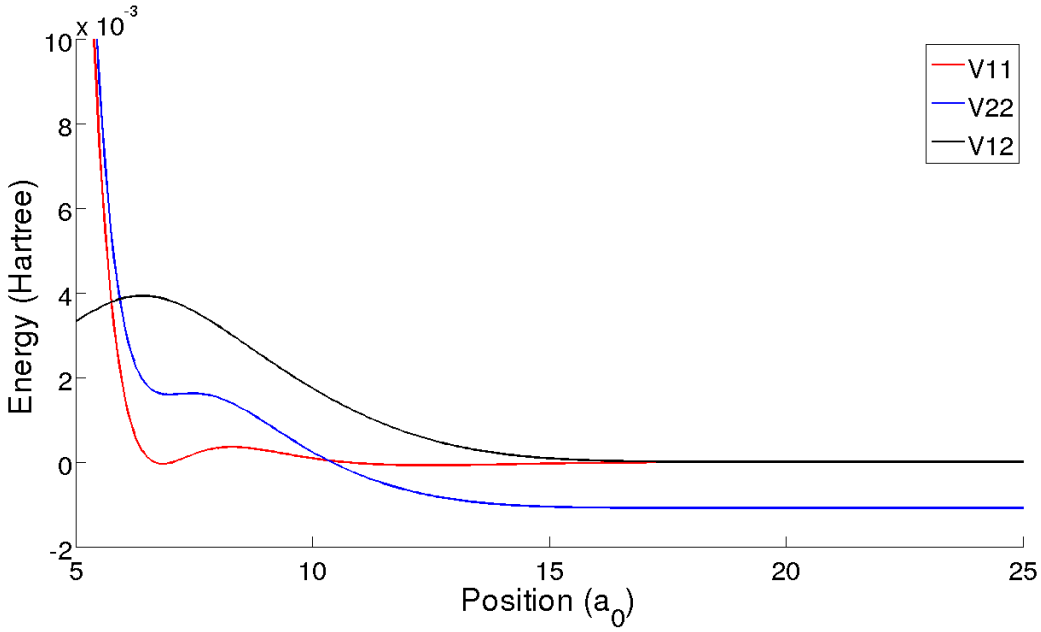

Figure 33. Potentials for Rb + Ar (diabatic representation).

lower in Rb + Ar, meaning the difference between W_Π and W_Σ surfaces is less, and therefore, according to Equation 41, the coupling is not as strong. Additionally, in the diabatic representation of Rb + Ar, there is a well present on both the $^2P_{3/2}$ and $^2P_{1/2}$ states, which is not present when compared to the Li + He surfaces.

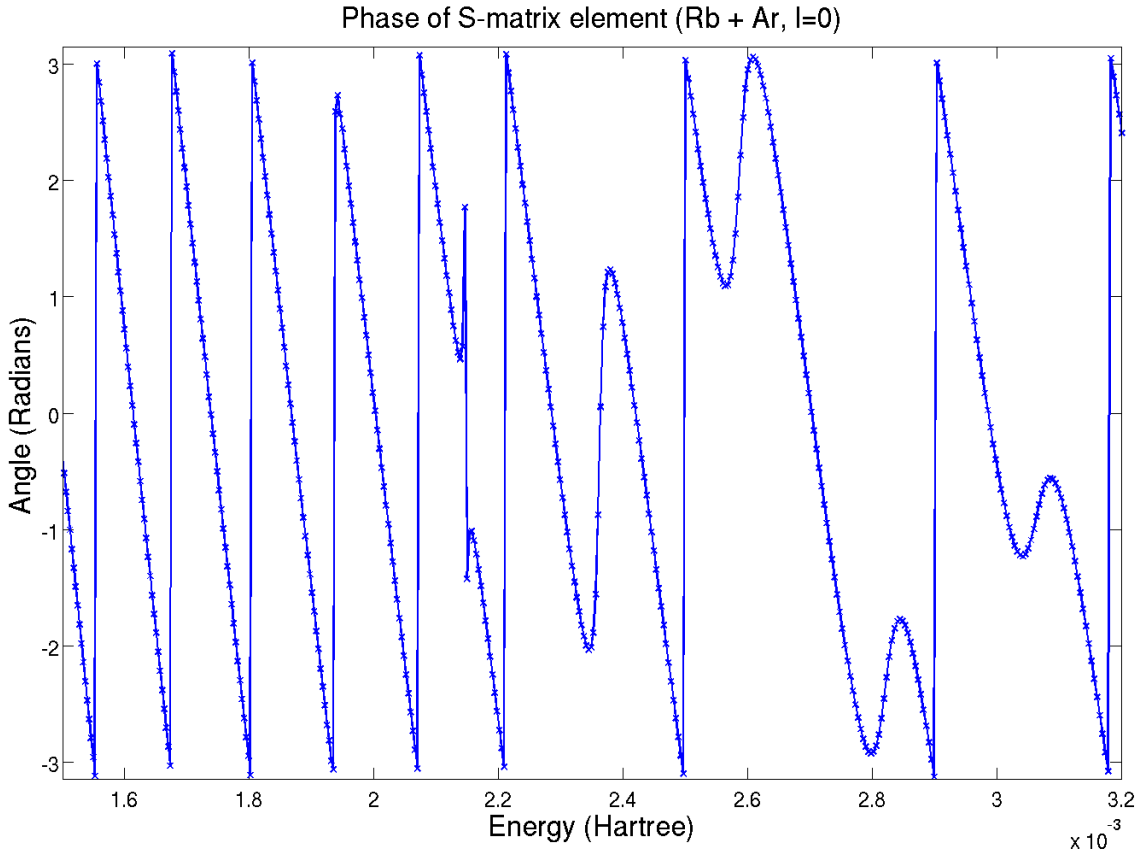

Figure 34. Real part of the phase of Rb + Ar scattering matrix for elastic scattering and no Centrifugal potential.

To investigate the possible influence of the presence of the well, the phase of the elastic S-matrix element for $l = 0$ (no Centrifugal potential term) is plotted in Figure 34. There appears to be some resonant structure associated with the wells which may be further inhibiting the transition between the fine structure states; further investigation is warranted.

In summary, the results obtained compare favorably to experimental results. Although two forms of coupling were neglected, the results were all within the proper order of magnitude, and were found to be close to experimental values. The results were also shown to exhibit proper behavior when extending to Rb + Ar, where the cross section is significantly lower. By examining the potentials and the time dependent behavior, it is possible to explain the low results for the Rb + Ar cross sections. Future work would include Coriolis and derivative coupling terms to more fully model the coupling between all states for Alkali + Noble Gas interactions, providing a more complete picture of the hyperfine state transitions.

5.7 Error Sources

There are four possible sources of error in these calculated cross sections, with the hypothesized most significant source of error listed first and the hypothesized least significant source of error listed last:

- The inputted adiabatic potentials
- The cutoff of the effective potential, particularly for larger Centrifugal potentials (larger l, and therefore higher energy)
- Numeric error arising from ensuring $|1 - S_{el}(k)|^2 \geq 0$, as discussed in Chapter IV
- Error in the discretization process

In particular, the results for Li + He were calculated using much higher quality potentials than the results for the other Alkali + Noble Gas combinations explored.

Since equally spaced points in k-space were used, higher energies contain fewer points, so the lack of significant shape in the high-energy regions may be due to

the smaller sampling in the high-energy region. This may be resolved by either using more data points or obtaining the Fourier transform of the correlation function (already obtained) at more energy values and using the analytic expression for a Gaussian for the Møller states. However, the rapid oscillations in the cross section calculations would be averaged out when convolving with a Boltzmann distribution, so the sampling error is relatively small.

VI. Conclusion

Code was written to calculate the absorption cross sections as a function of energy for two coupled one dimensional, spherically symmetric potentials. The Split Operator Method[4] was used to propagate the an initial Møller state, assumed to be a Gaussian in the asymptotic limit, through a potential. The correlation between the wave packet and Møller final state, which was also assumed to be a Gaussian when placed in the asymptotic limit, was calculated at each time step. Using the method of Tannor and Weeks[18], the correlation function was used to obtain scattering matrix elements. From scattering matrix elements for several different effective potential values and using the Method of Partial Waves[7], the absorption cross section is calculated. A method to estimate the algorithmic error was also developed.

6.1 General Method

The procedure developed to calculate absorption cross sections using the method of Tannor and Weeks[18] was developed. Through judicious choice of parameters, it was possible to obtain cross sections for several different energies. The procedure may be summed up as follows:

- Determine the energies to obtain scattering cross sections over
- Determine the k-values corresponding with those energies for the reduced mass of the system
- Position a Gaussian wave packet spanning those k-values in the asymptotic limit and propagate using the method in Chapter II for $l = 0$ to l_{max}
- Calculate the S-matrix elements for elastic and inelastic scattering

- By summing the magnitude of the S-matrix elements for elastic and inelastic scattering, determine the numerically stable region
- Calculate the absorption cross section using Equation (30)

The code for propagation and scattering was verified against several test cases to confirm correct behavior, as detailed in Chapter IV.

6.2 Results

It was determined that in order to use Gaussian Møller states, it was necessary to either position the initial wave packet very far away from the potential, or to truncate the effective potential beyond a certain point. For LiHe, since the computational time required to propagate for several different effective potentials would be prohibitive in the time available, the effective potential was truncated beyond 490 Bohr. This introduced some error which could be eliminated by either starting the packet farther out or by propagating the wave packet under the effective potential for each value of l from 0 to l_{max}.

Two different methods of coupling were examined. Under the first method, coupling was estimated from the spin-orbit split coupling. These results were analyzed for the high-quality Li + He surfaces, and produced results in the right ballpark, but the results were not extremely satisfying and could not be extended to other Alkali + Noble Gas potentials easily, since the spin-orbit split potentials for other combinations were not readily available.

Using a method discussed by Millard Alexander[2], it was possible to obtain a more satisfying diabatic potential representation from the W_Π and W_Σ surfaces. This method enabled examination of Li + ^{4}He, Li + ^{3}He, Na + ^{4}He, K + ^{4}He, and ^{85}Rb + Ar, assuming only radial coupling. The results in each case were slightly

below experimental results since derivative coupling and Coriolis coupling were both neglected. However, in each case, the cross section was close to experimental results. Furthermore, the substantial difference between Li + He and Rb + Ar was noticed, and some explanations from the dynamical propagation of the potentials were noted.

6.3 Future Work

There are several directions for future work stemming from thesis could go, but they can be boiled down to one of four main areas. First, there is a need to use the technique applied in this thesis, using different atomic systems with different potentials and compared to experimental data. The primary difficulty is obtaining reliable potentials for these systems.

Radial coupling was assumed to be the only coupling mechanism. One area of future work would be to relax this constraint and introduce Coriolis and/or derivative coupling terms. This should yield cross sections which are closer to the experimentally accepted values.

Another thrust of work stemming from this thesis would be development of a library of Møller initial and final states which are propagated out to infinity under the asymptotic Hamiltonian, then in to a reasonable point (perhaps 100 Bohr) under a Hamiltonian with the potential entirely due to the effective potential, for several different values of l. At a range of 100 Bohr, most atomic and molecular potentials have reached their asymptotic limits, but for large values of l necessary for the cross section calculations, the effective potential is still significant. Therefore, such a library would provide a better starting wave packet for future scattering calculations to be performed, independent of the atomic system, and reduce computational time required for one scattering calculation significantly – perhaps by as much as a factor of 2 or more. The savings in time is because by starting closer in space, the calcula-

tion does not have to extend as far in time. The results would also be more accurate, since a truncation of the effective potential would no longer be required. This would yield more accurate results than a truncation technique.

Finally, there are several inefficiencies in the code as presently written. The focus was on readable, working code and not on speed. It is possible that somewhat better performance could be obtained by cleaning up many of these inefficiencies. Although the performance would remain the same overall order of magnitude and is primarily limited by the FFT time, it is expected that a performance benefit of perhaps as much as a factor of 1.5 to 2 could be obtained by rewriting the code in a highly optimized manner. Some parameters are calculated that are not required for the scattering calculation and could be removed from optimized code. More details are provided in Appendix B.

Appendix A. Sample Input Data Files

There are three separate data files used to control the propagation, scattering, and cross section calculations. The files required are a Gaussian Wave Packet file (generally ending in .gauss), a Hamiltonian file (generally ending in .ham), and a Propagation file (generally ending in .prop). Each of these files, along with all possible options that are allowed, are discussed below.

In all data files, comments begin with the ! character, and blank lines are allowed. No spaces are allowed between the text label and the equal sign. All numeric inputs must be in atomic units.

1.1 Gaussian File

The Gaussian file is the simplest of all of the data files, and contains 4 required parameters. A sample Gaussian file is listed below:

```
! Position Gaussian Wave Packet on the left of the x grid
x0=40
! Spread in x-space. Note that dk0 = 1/(2*dx0)
dx0=0.8
! Moving to the left
k0=-4.2
! Reduced Mass of LiHe, in atomic units
mass=4677.23
```

The parameters are fairly self-explanatory, specifying a position, momentum, mass, and spread of the initial Gaussian wave packet. These parameters are used with Equation (17) to specify the initial wave packet. When performing a propagation with a Møller final state, the spread and mass are also used for the Møller final state automatically. The Gaussian file is required by the Propagator file.

1.2 Hamiltonian File

The Hamiltonian file contains an option for specifying whether or not to turn on the kinetic energy, as well as several options for the potential energy of either one or two state systems, and the interaction potential between these systems. Absorbing boundary conditions are also specified in the Hamiltonian file, as they are implemented as an imaginary modification to the diagonal elements of the potential. A sample Hamiltonian file is listed below:

```
! Hamiltonian data
! kinetic=none turns off the kinetic energy, for testing purposes only.
! kinetic=standard is implied if there is no kinetic= line in the file.
kinetic=standard

! Number of potentials
! If this parameter is not specified, then it is assumed there is only
! one potential.
num_potentials=2

! Set up first potential

! curr_potential tells the program which potential the data applies to
curr_potential=1

! potential= specifies the potential types.
! A full list of potential types is discussed later in this section.
! Here, a linear interpolation between data points is specified, with
! points found in the referenced file.
potential=interpolate
potential_filename=LiHe_dia_p32_full_17.dat

! Set up second potential
curr_potential=2
potential=interpolate
potential_filename=LiHe_dia_p12_full_17.dat

! Set up interaction potential between potential #1 and potential #2
! The parameters for a coupling potential are identical to parameters
! for an absorbing potential.
coupling=interpolate
```

```
coupling_filename=LiHe_dia_V12_full_17.dat

! Set up absorbing boundary conditions (optionally)
! boundary= sets the absorbing boundary condition type (currently,
! only gaussian or none is supported)
! If boundary=none or no specification is present, absorbing boundary
! conditions are disabled
boundary=gaussian
! It is possible to specify a large absorbing boundary conditions with
! magnitude greater than 1, although it is not usually necessary.
boundary_magnitude=1
! dx0 specifies the width of the Gaussian absorbing boundary condition.
boundary_dx0=10
```

Several different potentials are supported in addition to the linear interpolation. Any of these potentials can be used with either `potential=` or `coupling=`. Examples of each potential are given below. It is also possible to specify `potential=none` (or `coupling=none`) for no potential. When using two potentials, all potentials are specified in the *diabatic* representation.

The Hamiltonian file is required by the Propagator file.

1.2.1 Simple Harmonic Oscillator.

An example of a Simple Harmonic Oscillator potential specification is as follows:

```
potential=sho
potential_x0=0
potential_mass=0.5
potential_omega=1
```

These variables specify a potential of the form $\hat{V} = \frac{1}{2}m\omega^2(x-x_0)^2$. All parameters are required.

1.2.2 Square Well.

A square well potential may be specified, with different heights below, at, and above the well. The following code specifies a square potential:

```
! Potential energy
potential=square_well
! Start of the square well
potential_xmin=10
! End of the square well
potential_xmax=20
! The potential value inside the well
potential_height=-0.166
! With x < potential_xmin, the potential value
potential_lower=0
! With x > potential_xmax, the potential value
potential_upper=0
```

This sample sets a square well with a depth of 0.166 au inside the well, and no potential outside the well. All parameters are required to specify a square well potential.

1.2.3 Interpolation.

This performs a linear interpolation between each point in the data file specified. The parameters are as indicated in the first example in this section. There are two requirements for this data file:

- The data must contain two columns. The first column is the x (or r) value. The second column is the potential energy, in atomic units.
- The data must be sorted from least to greatest in the first column.

For x less than the first entry in the file, linear extrapolation is used, with the slope from the first entry used to extrapolate. For x greater than the last entry in

the file, linear extrapolation is used, with the assumption of no slope. (For spherical potentials, the potential should level off at some value.)

1.2.4 Morse and Lennard-Jones 6-12.

Morse and Lennard-Jones potentials were originally planned to be implemented, but were not implemented due to the difficulty in fitting the input potentials to a Morse or Lennard-Jones potential while maintaining accurate behavior. Therefore, use of the Morse or Lennard-Jones potentials have not been fully tested. It is recommended that the Linear Interpolation is used instead of the Morse or Lennard-Jones potentials, as it will allow a more arbitrary potential form.

1.3 Propagation File

The Propagator file combines the initial Gaussian wave packet, under some Hamiltonian, and discretized under further parameters as specified within the propagation file. An example of a Propagation file is as follows:

```
! Path from Propagator file to initial wave packet
gaussian=../LiHe_left.gauss
! Path from Propagator file to Hamiltonian file
hamiltonian=../LiHe_2p.ham

! Moller parameters are not required. If not specified, there
! is no Moller calculation, just a propagation.
! It is assumed the spread (dx0) and mass are the same. The
! Moller final state is assumed to be a Gaussian. The Moller
! initial state is assumed to be the initial wave packet.
moller_final_x0=50
moller_final_k0=4.2

! Set the packet and Moller final states, using potential numbers
! as in the Hamiltonian
! This is the elastic scattering case, so they are the same
! These parameters are not required, and default to 1 if not specified.
! Wave packet on the first potential
```

```
packet_potential=1
! Moller final state on the first potential
moller_potential=1

! Set l-value for effective potential modifications.
! If this parameter is not specified, the default is 0.
l_value=0
! Set cutoff position above which the effective potential is not applied.
! If this parameter is not specified, the default is 0
! (which means no cutoff).
l_max=490

! Directory to output resulting calculations to.
! This directory does *not* have to exist prior to execution
! WARNING: all data in this directory will be erased when the program
! is executed with this parameter file as input.
output_directory=out

! Other parameters for propagation:
! Number of data points to discretize the data set into
num_points=32768
! Minimum and maximum x-values
! NOTE: k-value data is only accurate when x_min=0. This is not a concern
! since the actual propagations are spherical potentials, where
! x_min=0 obviously.
x_min=0
x_max=320
! t_min=0 is assumed. That parameter may not be changed.
! Set the maximum time to propagate to
t_max=200000
! Set the step size in time
dt=1
```

Appendix B. Code Comments

2.1 Acknowledgements

The author is grateful to the developers of the Fastest Fourier Transform in the West library [12]. Additionally, the author is grateful to the developers of SCons version 1.2.0 [13], which was used to automate the program build process, and GCC 4.3 [1] (gfortran in particular), which was used to compile the program.

2.2 Code Availability

The code is available upon request from the author, who may be reached by e-mail at samuel.butler@us.af.mil, or from the author's thesis advisor, Dr. David Weeks.

The procedure in Chapter IV translates into the following for the user of the available code:

- Determine manually the required energies, Hamiltonian, wave packet, and base propagation parameters
- Create a .gauss, .ham, and .prop file based on this information (see Appendix A).
- Determine the tolerable lower bound on the error
- Run the following code to determine l_{max} and generate specific propagator files:

  ```
  $ prop_copy myfile.prop -n=1e-5
  ```

  (Alternatively, use -M=l_{max} to specify a user-defined maximum l-value.) *Several different propagator files will be generated ending with* .0 *to* .l_{max}.
- Propagate each file (except the original master file) and calculate S-matrix elements:

```
$ scattering myfile.prop.0 -n=1e-5
$ scattering myfile.prop.1 -n=1e-5
...
$ scattering myfile.prop.<l_max> -n=1e-5
```

(NOTE: By default, any propagation results in an outputted file each iteration. This may result in very large space requirements on your hard drive, and may result in substantially increased runtime. You may use -x=# or -k=# to control this output. If -x=0 or -k=0 is specified, only the initial and final packets are outputted. Using -x=1000 and -k=1000, for example, will output x and k only every 1000 iterations instead of the default of every iteration.)

- Run the following program to determine the cross sections:

```
$ xsection myfile.prop -n=1e-5
```

- Finally, use the cross-section data to calculate the collisional transfer rate manually by convolution of the absorption cross section with the Boltzmann distribution.

Additionally, a program named *propagator* is available. This program only performs the wave packet propagation, without calculating S-matrix elements.

2.3 Known Issues

On some platforms, it was noted that the scattering and xsection programs would result in a segmentation fault when outputting certain parameters to the screen. If a problem is encountered, do not run the affected program with the -s command-line option. The result of the program without using -s will appear silent, although the program will run as expected and will output results in the directory specified in the .prop file.

In the code used for the propagation, it is assumed that the initial wave packet is in the asymptotic Hamiltonian, outside of influence of the potential. Therefore, the Møller initial state is assumed to be the initial wave packet. Furthermore, this initial wave packet is assumed to be a Gaussian. The Møller final state is also assumed to be in the asymptotic Hamiltonian region, outside the influence of the potential, and therefore is also a Gaussian.

Command line options are consistent from one program to another, although not all programs will use all of the command-line options. This allows a user to specify one set of command-line options and simply pass those same options to each program being called.

This is the author's first major project in FORTRAN, and as such, there may be some hidden bugs or other issues that I am unaware of. It is known that the code is relatively inefficient. Some of the inefficiencies are due to calculations that are nice to have, but not essential, in calculating the cross sections. For example, the code verifies the wave packet has a projection of close to 1 at all iterations in time, if absorbing boundary conditions are not used. This redundancy is a good check to perform to identify numeric error, but is not fundamental to the calculation. As another example, the code calculates the expectation value in x and outputs this value to a file at all time steps. This information is also generally not needed, but enables some checks to ensure functioning code in certain situations. However, these calculations do not affect the order of magnitude of the runtime substantially.

If performance is especially sluggish, one of two major factors are likely to blame. If the number of data points in the discretization is specified in the parameter file as N, then for small N, the runtime will be limited by the I/O of data files to the hard drive for ψ and ξ at each point in time. To reduce this strain (and/or the amount of disk space consumed), use the -k=# and -x=# command line options to specify

outputs only every # iterations instead of the default of every iteration. If -k=0 or -x=0 is specified, only the initial and final wave packets are outputted. (The default is -k=0 and -x=0.)

At some point, a majority of the computational burden per iteration will shift to calculation of the FFT at each time step. To speed up an FFT-limited routine, use a smaller value of N. If this is not acceptable, then either increasing the time step or decreasing the maximum time will also enhance run time.

2.4 Disclaimer

The code from the author is provided as-is, with no guarantee, implied or stated, of working correctly. Although the author has much experience in programming in C and C++, this is the author's first major project in FORTRAN, and thus it is quite likely that there are amateur coding mistakes that may cause problems when porting the code to different platforms. The target operating system for this code is Linux; some changes are necessary in order to run the code on another operating system. The code was mostly written comply with the FORTRAN 95 standard, although some GCC extensions and FORTRAN 2003 features may have also been used.

The use of the code, in whole or in part, in the development of commercial software is strictly prohibited. It is provided strictly for free personal, academic, and government use only.

Bibliography

[1] *GNU Compiler Collection (version 4.3.3) [Online]*. Available: http://gcc.gnu.org [2009, Dec 15].

[2] Alexander, Millard H. "Adiabatic and approximate diabatic potential energy surfaces for the B-H_2 van der Waals molecule". *The Journal of Chemical Physics*, 99:6014–6026, 1993.

[3] Allard, Nicole and John Kielkopf. "The effect of neutral nonresonant collisions on atomic spectral lines". *Reviews of Modern Physics*, 54(4), October 1982.

[4] Alvarellos, J. and H. Metiu. "The evolution of the wave function in a curve crossing problem computed by a fast Fourier transform method". *The Journal of Chemical Physics*, 88:4957–4966, 1988.

[5] Blank, L. and David E. Weeks. "Private communication (pending publication)", 2009.

[6] Bransden, B. H. and C. J. Joachain. *Physics of Atoms and Molecules*. Prentice Hall, 2nd edition, 2003.

[7] Cohen-Tannoudji, Claude et al. *Quantum Mechanics*, volume 2. Wiley-Interscience, 2005. ISBN 978-0471164333.

[8] Cohen-Tannoudji, Claude et al. *Quantum Mechanics*, volume 1. Wiley-Interscience, 2005. ISBN 978-0471164333.

[9] Elward-Berry, Julianne and Michael J. Berry. "Lithium fine structure transitions induced by collisions with noble gas atoms". *The Journal of Chemical Physics*, 72:4500–4509, 1980.

[10] Faist, M. B. and R. B. Bernstein. "Computational study of elastic and electronically inelastic scattering of Br by ground state I atoms: Role of potential curve crossing". *The Journal of Chemical Physics*, 64:2971–2984, 1976.

[11] Faist, M. B. and R. D. Levine. "Collisional ionization and elastic scattering in alkali-halogen atom collisions". *The Journal of Chemical Physics*, 64:2953–2970, 1976.

[12] Frigo, M. and S. C. Johnson. *The Fastest Fourier Transform in the West (version 3.2.2) [Online]*. Available: http://www.fftw.org [2009, July 29].

[13] Knight, Steven et al. *SCons (version 1.2.0) [Online]*. Available: http://www.scons.org [2009, Dec 15].

[14] Lewis, Charlton D. "A theoretical model analysis of absorption of a three level diode pumped alkali laser". *Air Force Institute of Technology (Thesis)*, 2009.

[15] Nakamaya, Akira and Koichi Yamashita. "Path integral Monte Carlo study on the structure and absorption spectra of alkali atoms (Li, Na, K) attached to superfluid helium clusters". *The Journal of Chemical Physics*, 114:780–791, 2001.

[16] Reyes, A. and D. A. Micha. "Dynamics of spin-orbit recoupling in collisions of alkali atoms with noble-gas atoms using atomic core potentials". *The Journal of Chemical Physics*, 119:12316–12322, 2003.

[17] Rotondaro, M. D. "Collisional Dynamics of the Rubidium 5(2)P Levels". *Air Force Insitute of Technology (Dissertation)*, 1995.

[18] Tannor, David J. and David E. Weeks. "Wave packet correlation function formulation of scattering theory: The quantum analog of classical S-matrix theory". *Journal of Chemical Physics*, 98(5):3884, 1993.

[19] Townsend, John S. *A Modern Approach to Quantum Mechanics.* University Science Books, 2000. ISBN 1-891389-13-0.

[20] Verdeyen, Joseph T. *Laser Electronics.* Prentice Hall, 2002.

[21] Weeks, David E. "Private communication, based on Physics 756 Lecture Notes at the Air Force Institute of Technology, Wright-Patterson AFB, Ohio (unpublished)", 2009.

[22] Weeks, David E. and David J. Tannor. "A time-dependent formulation of the scattering matrix for the collinear reaction $H + H_2(\nu) \rightarrow H_2(\nu') + H$". *Chemical Physics Letters*, 224(5-6):451–458, 1994.

Vita

Captain Samuel Deaton Butler was born in Santa Clara, California. At the age of 12, he moved to his hometown of Twin Falls, Idaho. After graduating with honors from Twin Falls High School, he entered the United States Air Force on active duty as an Aircraft Communications and Navigation Systems Technician from June, 1998 to July, 2000, where he worked on the B-52H bomber and UH-1N helicopter at Minot Air Force Base, North Dakota. He was honorably discharged from active duty service as a Senior Airman in July, 2000 through the Airman Scholarship and Commissioning Program. Capt Butler then pursued bachelor's degree in Applied Physics with a Computer Science Emphasis at Brigham Young University (BYU) in Provo, Utah. He graduated with his Bachelor's Degree in Physics in April, 2004. Capt Butler was commissioned as an officer in the United States Air Force in April, 2004 through the Reserve Officer Training Corps (ROTC), Detachment 855, at BYU. Following ROTC, he re-entered active duty service and was assigned to the National Security Agency (NSA) at Fort George G. Meade, Maryland from June, 2004 to July, 2008. During that time, Capt Butler was detailed to the Pentagon on the Global Hawk program under the Secretary of the Air Force's Acqusitions (SAF/AQ) for 6 months. Following his duties at SAF/AQ, Capt Butler then served as a squadron Executive Officer for the 29th Intelligence Squadron at Fort George G. Meade for 6 months. In August, 2005, he was assigned to the NSA Research Directorate where he supported fundamental research at the Advanced Research and Development Activity (ARDA). After working in research, he worked in the Signals Intelligence Directorate. Capt Butler entered graduate school at the Air Force Institute of Technology (AFIT) in August of 2008 and he is currently completing his Master's Degree.

REPORT DOCUMENTATION PAGE

Form Approved
OMB No. 0704–0188

1. REPORT DATE *(DD–MM–YYYY)*	2. REPORT TYPE	3. DATES COVERED *(From — To)*
25–03–2010	Master's Thesis	Aug 2008 — Mar 2010

4. TITLE AND SUBTITLE

Calculation of Collisional Cross Sections for the $^2P_{3/2} \rightarrow {}^2P_{1/2}$ Transition in Alkali-Noble Gas Systems

5a. CONTRACT NUMBER

5b. GRANT NUMBER

5c. PROGRAM ELEMENT NUMBER

6. AUTHOR(S)

Butler, Samuel D., Capt, USAF

5d. PROJECT NUMBER

5e. TASK NUMBER

5f. WORK UNIT NUMBER

7. PERFORMING ORGANIZATION NAME(S) AND ADDRESS(ES)

Air Force Institute of Technology
Graduate School of Engineering and Management (AFIT/EN)
2950 Hobson Way
WPAFB OH 45433-7765

8. PERFORMING ORGANIZATION REPORT NUMBER

AFIT/GAP/ENP/10-M04

9. SPONSORING / MONITORING AGENCY NAME(S) AND ADDRESS(ES)

High-Energy Laser Joint Technology Office
901 University Blvd SE Ste 100
Albuquerque, NM 87106
(505) 248-8208, harro.ackerman@jto.hpc.mil

10. SPONSOR/MONITOR'S ACRONYM(S)

HEL JTO

11. SPONSOR/MONITOR'S REPORT NUMBER(S)

12. DISTRIBUTION / AVAILABILITY STATEMENT

APPROVED FOR PUBLIC RELEASE; DISTRIBUTION UNLIMITED.

13. SUPPLEMENTARY NOTES

14. ABSTRACT

Collisional cross sections were calculated as a function of energy for two coupled one dimensional, spherically symmetric potentials. The Split Operator Method was used to propagate an initial Møller state, chosen to be a Gaussian in the asymptotic limit, through a potential. The correlation between the wave packet and Møller final state was calculated at each time step. Using the Channel Packet Method, the correlation function was used to obtain scattering matrix elements. From scattering matrix elements for several different effective potential values and using the Method of Partial Waves, the collisional cross section is calculated for the transition from the $^2P_{3/2}$ to $^2P_{1/2}$ level. This method was applied to LiHe at low energy, with results close to experimentally measured values for Alkali-Noble Gas interactions. Cross sections were also calculated for NaHe, KHe, RbAr, and LiHe-3. An explanation for the low RbAr cross sections from the time dependent calculations is provided.

15. SUBJECT TERMS

Channel Packet Method, Collision, Alkali, Noble Gas, Cross Section, Partial Waves, Scattering, Time Dependent, Li, Na, K, Rb, He, Ar

16. SECURITY CLASSIFICATION OF:			17. LIMITATION OF ABSTRACT	18. NUMBER OF PAGES	19a. NAME OF RESPONSIBLE PERSON
a. REPORT	b. ABSTRACT	c. THIS PAGE			Dr. David E. Weeks
U	U	U	UU	107	19b. TELEPHONE NUMBER *(include area code)* (937) 255-3636, x4561; david.weeks@afit.edu